





41 Continent pose significant challenges, as indicated by higher monthly AOD root mean square  
42 error. Moreover, regions that are distant from major aerosol source areas, including the polar  
43 regions, and remote oceans exhibit large relative differences in speciated AODs and fine-mode vs  
44 coarse-mode AODs among the four reanalyses. To ensure consistency across the globe, a multi-  
45 reanalysis-consensus (MRC) approach was developed similar to the International Cooperative for  
46 Aerosol Prediction Multi-Model Ensemble (ICAP-MME). Like the ICAP-MME, while the MRC  
47 does not consistently rank first among the reanalyses for individual regions, it performs well by  
48 ranking first or second globally in AOD correlation and RMSE, making it a suitable candidate for  
49 climate studies that require robust and consistent assessments.

50

51 Keywords: Aerosol, Reanalysis, Aerosol Optical Depth, intercomparison, ICAP-MME

52

53 Short Summary

54 The study compares and evaluates the monthly aerosol optical depth of four reanalyses (RA) and  
55 their consensus. The basic verification characteristics of these RA versus both AERONET and  
56 MODIS retrievals are presented. The study discusses the strength of each RA and identifies regions  
57 where diversity and challenges are prominent. The RA consensus usually performs very well on a  
58 global scale in terms of how well it matches the observational data, making it a good choice for  
59 various applications.

60



61 1. Introduction

62 In recent years, global aerosol reanalyses have been developed by major operational and research  
63 centers, owing to the availability of long-record satellite remote sensing aerosol products and  
64 advancements in aerosol data assimilation and modeling. These reanalyses are based on their  
65 operational counterparts that are included in the "Core Four" members of the International  
66 Cooperative for Aerosol Prediction Multi Model Ensemble (ICAP-MME C4C; Sessions et al.,  
67 2016; Xian et al., 2019; Reid et al., 2022). The reanalyses include the Copernicus Atmosphere  
68 Monitoring Service ReAnalysis (CAMSR; Inness et al., 2019) produced by the European Centre  
69 for Medium-Range Weather Forecasts (ECMWF); the Japanese Reanalysis for Aerosol (JRAero)  
70 (Yumimoto et al., 2017) developed by the Japan Meteorological Agency (JMA); the NASA  
71 Modern-Era Retrospective Analysis for Research and Applications, version 2 (MERRA-2;  
72 Randles et al., 2017); and the Navy Aerosol Analysis and Prediction System reanalysis (NAAPS-  
73 RA; Lynch et al., 2016) developed by the U.S. Naval Research Laboratory (NRL).

74 The aerosol reanalyses are similar to their operational counterparts and characterized by a high  
75 degree of independence in their underlying meteorology, aerosol sources, sinks, microphysics, and  
76 chemistry, as well as in their assimilation methods for aerosol optical depth (AOD) observations.  
77 A summary of the configurations of these four reanalyses is presented in Table 1. Notably, the use  
78 of operational Terra and Aqua Moderate Resolution Imaging Spectrometer data (MODIS Dark  
79 Target and Deep Blue; Levy et al., 2013; Hsu et al., 2013) is consistent across these reanalyses,  
80 although preprocessing treatments vary. These treatments include quality control, bias correction,  
81 and aggregation and sampling. Additionally, several other products, such as MultiAngle Imaging  
82 Spectroradiometer (MISR; Kahn et al., 2010), Advanced Very High Resolution Radiometer  
83 (AVHRR; e.g., Ignatov et al., 2002), and Polar Multi-Sensor Aerosol product (PMAp; Grzegorski  
84 et al., 2022), are assimilated into some of these reanalyses. Therefore, between their underlying  
85 meteorology, physics, and data assimilation these reanalyses are characterized by a high degree of  
86 independence overall.

87 Like atmospheric reanalysis products, aerosol reanalysis products, whether used individually or in  
88 combination, have been employed for diverse applications. They provide comprehensive aerosol  
89 climatology and statistics to aid in understanding aerosol conditions across various regions and the  
90 world (e.g., Reid et al., 2012; Xian et al., 2020; Nignombam et al., 2021; Ohno et al., 2022; Rubin  
91 et al., 2023). They are widely used to address a multitude of scientific inquiries in the fields of  
92 aerosol radiative forcing (e.g., Randles et al., 2017; Markowicz et al., 2017; 2021a,b; Ohno et al.,  
93 2022; Zhang et al., 2023), aerosol-cloud interaction (e.g., McCoy et al., 2017; Ross et al., 2018;  
94 Eck et al., 2018), aerosol-cryosphere interaction (e.g., Khan et al., 2018, 2019; 2020;  
95 Roychoudhury et al., 2022), air quality and its impact on health (e.g., Tong et al., 2023; Cui et al.,  
96 2022; Jenwitheesuk et al., 2022; Lacima et al., 2022), biogeochemical cycles (e.g., Rahav et al.,  
97 2020; Borchardt et al., 2019; Mescioglu et al., 2019), among others. These reanalyses have been  
98 rigorously evaluated by the developing centers and various studies from different perspectives,  
99 including AOD and other aerosol optical properties, mass concentrations, and vertical distribution  
100 profiles. However, to date, no intercomparison among the four reanalyses has been conducted.

101 This study presents an intercomparison of the four available global aerosol reanalyses to evaluate  
102 their skill in simulating monthly average AOD. Additionally, this study includes the development  
103 of a Multi Reanalysis Consensus (MRC) product using a multi-model-consensus approach, similar



104 to the ICAP Multi Model Ensemble (ICAP-MME; Sessions et al., 2015; Xian et al., 2019). The  
105 MRC is a consensus mean of the four individual reanalyses, with a spatial resolution of  $1^\circ \times 1^\circ$   
106 latitude/longitude and monthly temporal resolution. The study provides speciated AODs, fine-  
107 mode (FM), coarse-mode (CM) and total AODs at 550 nm for the period of 2003-2019 from three  
108 reanalyses, and all four reanalyses are available for the time period of 2011-2019. In addition, a  
109 companion study focuses on global and regional AOD trends derived from these reanalyses. The  
110 validation of AODs from the MRC, and the four component members, is performed using ground-  
111 based AEROSol Robotic NETwork (AERONET; Holben et al., 1998) observations, with MODIS  
112 AOD for spatial distribution evaluation. The validation results, as well as the AOD climatology  
113 and diversity of the reanalyses, are presented in Section 3. The study concludes with a summary  
114 of the findings in Section 4.

115

## 116 2. Data and Methods

117 This study intercompares the monthly average modal (total, FM, and CM) and speciated AOD  
118 products from four aerosol reanalyses (RA) and their consensus, and evaluates the RA AODs with  
119 AERONET and the combined MODIS Dark Target/Deep Blue retrievals (Levy et al., 2013).

### 120 2.1 Individual product lines

121 Descriptions of the four reanalysis datasets, including CAMSRA, JRAero, MERRA-2, and  
122 NAAPS-RA v1, are provided in this section. Table 1 provides a summary of the features of the  
123 four reanalyses and the MRC used in this study.

#### 124 2.1.1 CAMSRA

125 The Copernicus Atmosphere Monitoring Service (CAMS) Reanalysis (CAMSRA, Inness et al.,  
126 2019) is run at the European Centre for Medium-Range Weather Forecasts (ECMWF) and is a  
127 global reanalysis of atmospheric composition species, including aerosols. It builds on the  
128 previous reanalyses of the MACC project (Inness et al., 2013) and the CAMS interim reanalysis  
129 (Flemming et al., 2017). The CAMSRA is publicly available for the years 2003 to 2022 and is  
130 being continuously updated for future years.

131 The CAMSRA is based on the Integrated Forecasting System (IFS) used by ECMWF for  
132 numerical weather prediction and meteorological reanalysis. Two additional modules are  
133 incorporated into the IFS for the CAMSRA, one to calculate the processes and reactions of the  
134 chemical species and one to represent the prognostic aerosol species. The aerosol scheme  
135 includes prescribed and online emissions, dry and wet deposition, production of sulfate from a  
136 gas-phase sulfur dioxide precursor, and the aging of hydrophobic organic matter and black  
137 carbon to hydrophilic. The prescribed anthropogenic emissions come from the MACCcity  
138 inventory (Granier et al., 2011) and the biomass burning (BB) emissions from the Global Fire  
139 Assimilation System, version 1.2 (GFASv1.2) (Kaiser et al., 2012). GFASv1.2 is a separate  
140 system to the IFS that uses satellite retrievals of fire radiative power to produce the BB emissions  
141 that are then input as fixed emissions to the aerosol scheme. The transport of the aerosol species



142 by advection, convection and diffusion is calculated using the meteorological component of the  
143 IFS and the wind fields from the meteorology are also used as parameters to estimate the online  
144 sea salt (Monahan et al., 1986) and dust (Ginoux et al., 2001) surface emissions. One key  
145 difference between the CAMSRA set up of the IFS and that used for numerical weather  
146 prediction, is that for the CAMSRA the radiative impact of aerosol particles and ozone on  
147 meteorology is also accounted for.

148 The observations used in the CAMSRA for aerosols are of total AOD at 550nm. These come  
149 from MODIS collection 6 satellite retrievals for the entire period covered by CAMSRA and from  
150 the Advanced Along-Track Scanning Radiometer for the period 2003-2012. These AOD  
151 observations are simultaneously assimilated with trace gas and meteorological observations  
152 using the 4D variational data assimilation system of the IFS with a 12-hour assimilation window.  
153 The products available from the CAMSRA include speciated AODs at a 3-hour temporal and  
154 approximately 0.7 degrees spatial resolution, whereas monthly mean AODs at 550nm were used  
155 in this study.

#### 156 2.1.2 JRAero

157 The Japanese Reanalysis for Aerosol (JRAero) was developed by the Meteorological Research  
158 Institute (MRI) of the Japan Meteorological Agency and Kyushu University using the global  
159 aerosol transport model MASINGAR Mk-2 (Yukimoto et al., 2012) and a two-dimensional  
160 variational (2D-Var) data assimilation method. The model uses the MRI-AGCM3 atmospheric  
161 general circulation model, and considers major tropospheric aerosol components, including black  
162 carbon (BC), organic carbon (OC), mineral dust, sea salt, and sulfate aerosols, and their precursors.

163 JRAero assimilates global AOD from a bias-corrected MODIS Level 3 AOD product provided by  
164 the US Naval Research Laboratory (NRL) and the University of North Dakota  
165 (<http://doi.org/10.5067/MODIS/MCDAODHD.NRT.061>) every 6 hours. Anthropogenic and  
166 biomass burning emissions were estimated using the MACCity (MACC/CityZEN EU projects)  
167 emission inventory ([http://accent.aero.jussieu.fr/MACC\\_metadata.php](http://accent.aero.jussieu.fr/MACC_metadata.php)) and the Global Fire  
168 Assimilation System (GFAS) dataset ([http://www.gmes-atmosphere.eu/about/project\\_structure/input\\_data/d\\_fire](http://www.gmes-atmosphere.eu/about/project_structure/input_data/d_fire)). The reanalysis has a resolution of  
169 TL159 (about  $1.1^\circ \times 1.1^\circ$ ) with 48 vertical layers from the ground to 0.4 hPa. Validation results  
170 and additional information can be found in Yumimoto et al. (2017).  
171

#### 172 2.1.3 MERRA-2

173 The NASA Modern-Era Retrospective Analysis for Research and Applications, version 2  
174 (MERRA-2, Gelaro et al. 2017) is an atmospheric and aerosol reanalysis produced with the  
175 NASA Goddard Earth Observing System (GEOS) Earth system model. Aerosol data assimilation  
176 brings in data from the MODIS and MISR satellite sensors (after 2000) and includes AERONET  
177 ground-based sun photometer observations (through 2014). The Goddard Chemistry, Aerosol,  
178 Radiation, and Transport model (GOCART; Chin et al. 2000; Colarco et al. 2010) is run online  
179 and radiatively coupled in the MERRA-2 system, and provides simulations of dust, sea salt,  
180 sulfate, and black and organic carbon aerosol species.



181 Black and organic carbon are each partitioned into hydrophobic and hydrophilic modes, and a  
182 single bulk sulfate aerosol species is carried. Dust and sea salt are partitioned into five non-  
183 interacting size bins, with dust emissions based on the model 10-m wind speed and a topographic  
184 source function following Ginoux et al. (2001), and sea salt emissions driven by the surface wind  
185 friction speed modified from Gong (2003) and with a sea-surface temperature adjustment based  
186 on Jaeglé et al. (2011). Explosive volcanic sulfur emissions are included through 2010 based on  
187 Diehl et al. (2012), with a repeating annual cycle of degassing volcanic emissions subsequent.  
188 Other emissions are as summarized in Table 1.

189 The analysis of AOD is performed on quality-controlled MODIS, MISR, and AERONET data as  
190 described in Randles et al. (2017) and Buchard et al. (2015). The AOD analysis is performed by  
191 means of analysis splitting, where first a 2-D analysis of AOD is performed using error  
192 covariances derived from innovation data. Three-dimensional analysis increments for aerosol  
193 mass concentration are then computed using the Local Displacement Ensemble (LDE)  
194 methodology, which accommodates misplacement of the aerosol plumes due to source or  
195 transport issues. The ensemble perturbations are generated at the full model resolution, without  
196 the need for multiple model runs. Online quality control is performed as in Dee et al. (2001),  
197 with observation and background errors estimated as in Dee and da Silva (1999). Randles et al.  
198 (2017) and Buchard et al. (2017) describe the overall methodology and validation of the  
199 MERRA-2 AOD reanalysis. For this study, monthly mean speciated AODs and total AOD at 550  
200 nm with 0.5 degree latitude and 0.625 degree longitude spatial resolution were used.

#### 201 2.1.4 NAAPS-RA v1

202 The Navy Aerosol Analysis and Prediction System (NAAPS, Lynch et al., 2016) is a global offline  
203 chemical transport model developed at the U.S. Naval Research Laboratory. NAAPS simulates the  
204 life cycles of aerosol particles and their gaseous precursors. The particle species include  
205 anthropogenic and biogenic fine (ABF, a mix of sulfate, organic aerosols and BC from non-BB  
206 sources), BB smoke, aeolian dust, and sea salt aerosols. The transport, hygroscopic growth of  
207 particles, dry and wet removal processes of these particles, and emissions of wind-blown particles  
208 are driven by the meteorological fields from the Navy Global Environmental model (NAVGEN,  
209 Hogan, et al., 2014). Secondary organic aerosol (SOA) processes are represented with a 1<sup>st</sup> order  
210 approximation method, in which production of SOA from its precursors is assumed to be instant  
211 and is pre-treated outside the model. Anthropogenic emissions come from the MACC inventory  
212 from ECMWF (Granier et al., 2011). BB smoke emission is derived from the Fire Locating and  
213 Modeling of Burning Emissions (FLAMBE, Reid et al., 2009), which is constructed based on the  
214 MODIS fire hot spot data. In the reanalysis version, additional orbital corrections and regional  
215 emission factors are incorporated. Aeolian dust emissions are determined based on the surface  
216 friction velocity to the fourth power, and surface erodibility, which is adopted from Ginoux et al.  
217 (2001) with regional tuning. Dust emission occurs when specific conditions related to surface  
218 wetness and friction velocity thresholds are met. The representation of sea spray process adheres  
219 to Witek et al. (2007), with sea salt emission being governed by sea surface wind conditions.



220 The NAAPS-ReAnalysis (NAAPS-RA) v1 (Lynch et al., 2016) is derived from NAAPS, with  
 221 assimilation of quality-assured and quality-controlled MODIS (Zhang et al., 2006; Hyer et al.  
 222 2011) and MISR AOD products (Shi et al., 2011) using 2D variational data assimilation method  
 223 (Zhang et al., 2008). It provides 3-D mass concentration, extinction, and 2-D 550 nm AOD from  
 224 these aerosol species with 1°x1° latitude/longitude spatial and 6-hourly temporal resolution for the  
 225 years 2003-2022. The BB smoke source and dust sources are regionally tuned to best match the  
 226 FM and CM AODs with AERONET AODs. Aerosol wet removals within the tropical region were  
 227 regulated with satellite precipitation product (Xian et al., 2009) to mitigate model's deficiency to  
 228 simulate convective precipitation. The reanalysis shows similar decadal trend of AOD found in  
 229 satellite products (e.g., Zhang et al., 2017) and was verified with various field campaign data (e.g.,  
 230 Reid et al., 2016; Atwood et al., 2017; Edwards et al., 2022; Reid et al., 2023) in addition to ground  
 231 and space-based observations.

## 232 2.2 Multi-reanalysis-consensus (MRC)

233 The MRC product is a result of combining four individual aerosol reanalysis products described  
 234 above. This method follows the multi-model-ensemble approach used by the International  
 235 Cooperative for Aerosol Prediction (ICAP) and is based on the work by Sessions et al. (2015) and  
 236 Xian et al. (2019). The MRC provides speciated and total AOD at 550 nm with a 1°x1° lat/lon  
 237 degree and monthly resolution for the period 2011-2019. Data for the period 2003-2010 are  
 238 available from all three individual reanalyses except JRAero.

239 Table 1. Summary of the characteristics of the aerosol reanalyses.

	Organization	Meteorology	Resolution lat x lon	DA metho	Assimilated obs.	Species	Anthro. & Biogenic Emission	BB Emissions	Available time	reference
CAMSRA	ECMWF	Inline ERA5	0.7 x 0.7	4D-Var	DAQ MODIS PMAp	BC, OM, Sulfate Dust, Sea Salt	MACCity (trend: ACCMIP + RCP8.5), monthly VOC	GFAS	2003-present	Inness et al., 2019
MERRA-2	NASA	Inline MERRA-2	0.5 x 0.6	2D-Var +LDE	Neural Net MODIS, MISR, AVHRR, AERONET	BC, OC, Sulfate Dust, Sea Salt	EDGAR V4.1, AeroCom Phase II	GFED before 2009, QFED after 2009	1980-present	Randles et al., 2017
NAAPS-RA	NRL	Offline NOGAPS/NAVGEN	1 x 1	2D-Var	DAQ MODIS, MISR	BB smoke, Dust, Sea Salt, ABF	MACCity, BOND POET, monthly SOA	FLAMBE	2003-present	Lynch et al., 2016
JRAero	JMA	Inline MRI AGCM3	1.1 x 1.1	2D-Var	DAQ MODIS	BC, OC, Sulfate Dust, Sea Salt	MACCity	GFAS	2011-present	Yumimoto et al., 2017
MRC	-	-	1 x 1	-	-	BB smoke, Dust, Sea Salt, ABF	-	-	2003-present	this work

## 241 2.3 AERONET

242 AERONET is a global ground-based sun photometer network managed by NASA. Sun and sky  
 243 radiance at multiple wavelengths, covering the near-ultraviolet to near-infrared, are measured  
 244 (Holben et al., 1998). Version 3 Level 2 AERONET daily data (Giles et al., 2019), which are  
 245 cloud-screened and quality-assured, are used in this study. The estimated uncertainty in  
 246 AERONET measured AOD, due primarily to calibration uncertainty, is ~0.01-0.02 at optical  
 247 airmass of one for network field instruments (with the highest errors in the UV; Eck et al., 1999).

248 The 550 nm FM and CM AODs and total AODs are derived with the Spectral Deconvolution  
 249 Method (SDA; O'Neill et al. 2003). The AERONET SDA product has been verified using in situ  
 250 measurements (see for example Kaku et al., 2014). The spectral separation of FM and CM particles  
 251 is determined based on their distinctive optical properties and complete size distributions. As part  
 252 of this separation, a diameter of approximately 1µm serves as an approximate threshold to



253 differentiate FM and CM particles. This optical separation is different from the sub-micron fraction  
254 (SMF) method that uses a specified cutoff radius of the particle size distribution in the AERONET  
255 (AOD & sky radiance) inversion and allows more data to be available compared to the SMF  
256 method. The FM fraction based on SDA is generally comparable and slightly greater than SMF  
257 (O'Neill et al., 2023).

258 This study uses AERONET sites that have more than 5 years of observations and more than 1000  
259 daily data between 2011 and 2019 for verification purposes. Monthly AOD was derived for months  
260 that have more than 15 days of daily data. Then only sites with more than 45 total number of  
261 months (upper three quartiles of sites regarding total number of monthly data) were selected. This  
262 resulted in a total number of 200 sites globally. A list of the site names is available in Table S1  
263 and locations of these sites can be found in Figure 8.

#### 264 2.4 MODIS AOD

265 MODIS AOD, used for global AOD distribution evaluation of the RAs, was based on Collection  
266 6.1 Dark Target and Deep Blue retrieval products (Levy et al., 2013). Additional quality control  
267 processes were applied as described in Zhang and Reid (2006) and Shi et al. (2011) for over water,  
268 Hyer et al. (2011) for over land, and Shi et al. (2013) for over desert regions. These quality control  
269 processes were updated for the Collection 6.1 data and the final MODIS C6.1 AOD (550 nm) data  
270 is a level 3 product with  $1^\circ \times 1^\circ$  latitude/longitude spatial and 6-hourly temporal resolution. Those  
271 6-hour-averaged MODIS AOD data were then binned into monthly means. Note that MODIS  
272 AOD products are well known to low bias significant aerosol events (Reid et al., 2022; Gumber et  
273 al., 2023), which could result in a slightly low AOD climatology, especially in source regions.

#### 274 2.5 Analysis Method

275 This study aims to investigate the diversity and utility of RAs for climate-scale studies by exploring  
276 the AOD at 550 nm. To achieve this goal, the AOD data from the RAs, as well as MODIS, were  
277 spatially and temporally binned into  $1^\circ \times 1^\circ$  degrees and monthly resolutions. For the purpose of  
278 verification and intercomparison analysis, only the data between 2011 and 2019 were used as that  
279 is the time period when all the RAs have data. The study focuses on the 550 nm AOD parameter  
280 since it is available for all the four aerosol RAs and MODIS. Furthermore, the AERONET FM and  
281 CM AODs at 550 nm were obtained using the SDA method described in Sect. 2.3.

282 The study examines the performance of RAs globally and regionally. Sixteen regions, including  
283 the globe, are defined for regional aerosol property analysis. They include East Asia, Southeast  
284 Asia, South Asia, Maritime Continent, Australia, Southwest Asia, Europe, Northwest Africa,  
285 South Africa, West North America, East North America, Central America, South America, as  
286 indicated by the rectangular boxes in Figure 5, and Arctic (north of  $70^\circ\text{N}$ ), and Antarctic (south of  
287  $75^\circ\text{S}$ ). There is no AERONET site satisfying site selection criteria as described in Section 2.3  
288 in the Arctic and Antarctic, so these two regions are not included for regional verification though  
289 they are included in other analyses.

290 Regarding the aerosol species, the study focuses on BB smoke, ABF in NAAPS-RA, and its  
291 equivalent of sulfate for MERRA-2, CAMSRA, and JRAero, as well as dust and sea salt. The



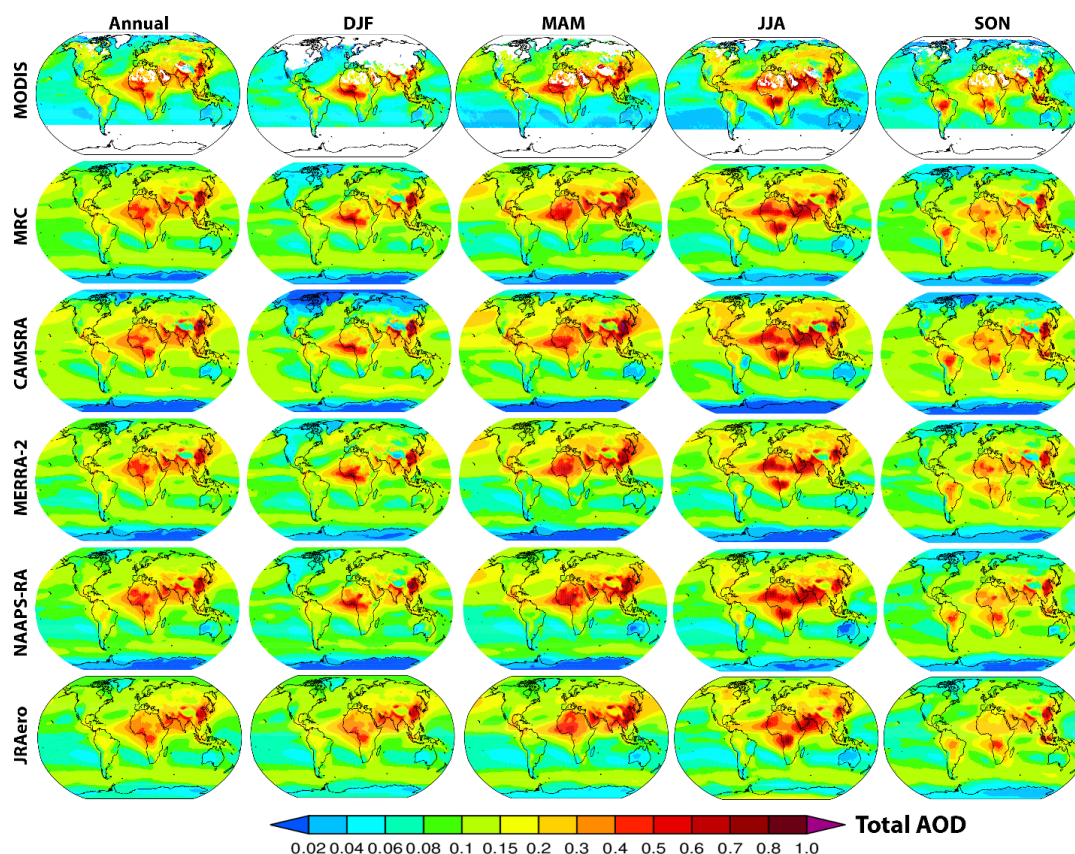
292 definition of species follows the ICAP practices (Sessions et al., 2015; Xian et al., 2019) for the  
293 operational counterparts of these RAs and previous applications of these RAs (e.g., Xian et al.,  
294 2022), in which the sum of Organic Matter (OM) and BC AODs from CAMSRA, and the sum of  
295 OC and BC AODs from MERRA-2 and JRAero, is used to approximate BB smoke AODs.  
296 Although this separation of species may be somewhat arbitrary, the study takes into account the  
297 fact that different aerosol types and sources may be represented differently in each RA. For  
298 example, the NAAPS-RA model characterizes aerosol species by emission source rather than  
299 chemical speciation, which makes it unique. In contrast, CAMSRA, MERRA-2, and JRAero  
300 characterize OM or OC, BC, and inorganic species, merging contributions from various  
301 anthropogenic, biomass burning and biogenic sources.

302 The study also assumes that all sea salt and dust are CM, while other aerosol species are FM. The  
303 segregation of sea salt and dust to the CM category is based on the fact that only a small portion  
304 of total sea salt or dust AOD at 550nm are attributed to their FM components. For example, FM  
305 sea salt represents about 17%, 10% and 11% of total sea salt AOD globally in MERRA-2,  
306 CAMSRA and JRAero respectively. The numbers are about 30%, 39% and 32% for dust. While  
307 FM fraction of dust during dust storms in Africa varies between 20-25% according to AERONET.  
308 The FM fraction of dust from MERRA-2, CAMSRA and JRAero might be biased high as these  
309 global models tend to overestimate FM dust and underestimate CM dust (for example O'Sullivan  
310 et al., 2020; Kramer et al., 2020). In contrast, NAAPS-RA assumes all sea salt and dust are CM.  
311 Verification results based on the FM and CM AODs derived using the FM fractions of sea salt and  
312 dust from MERRA-2, CAMSRA and JRAero can be found in the supplemental material.  
313 Generally, the validation of FM and CM AODs with AERONET data shows a degradation in  
314 performance for the three RAs compared to the verification results presented below.

315 AOD validation results for total, FM, and CM AOD regarding bias, root mean square error  
316 (RMSE), and coefficient of determination ( $r^2$ ) for monthly-mean AODs are presented.

### 317 3. Results

#### 318 3.1 Total and speciated AOD climatology



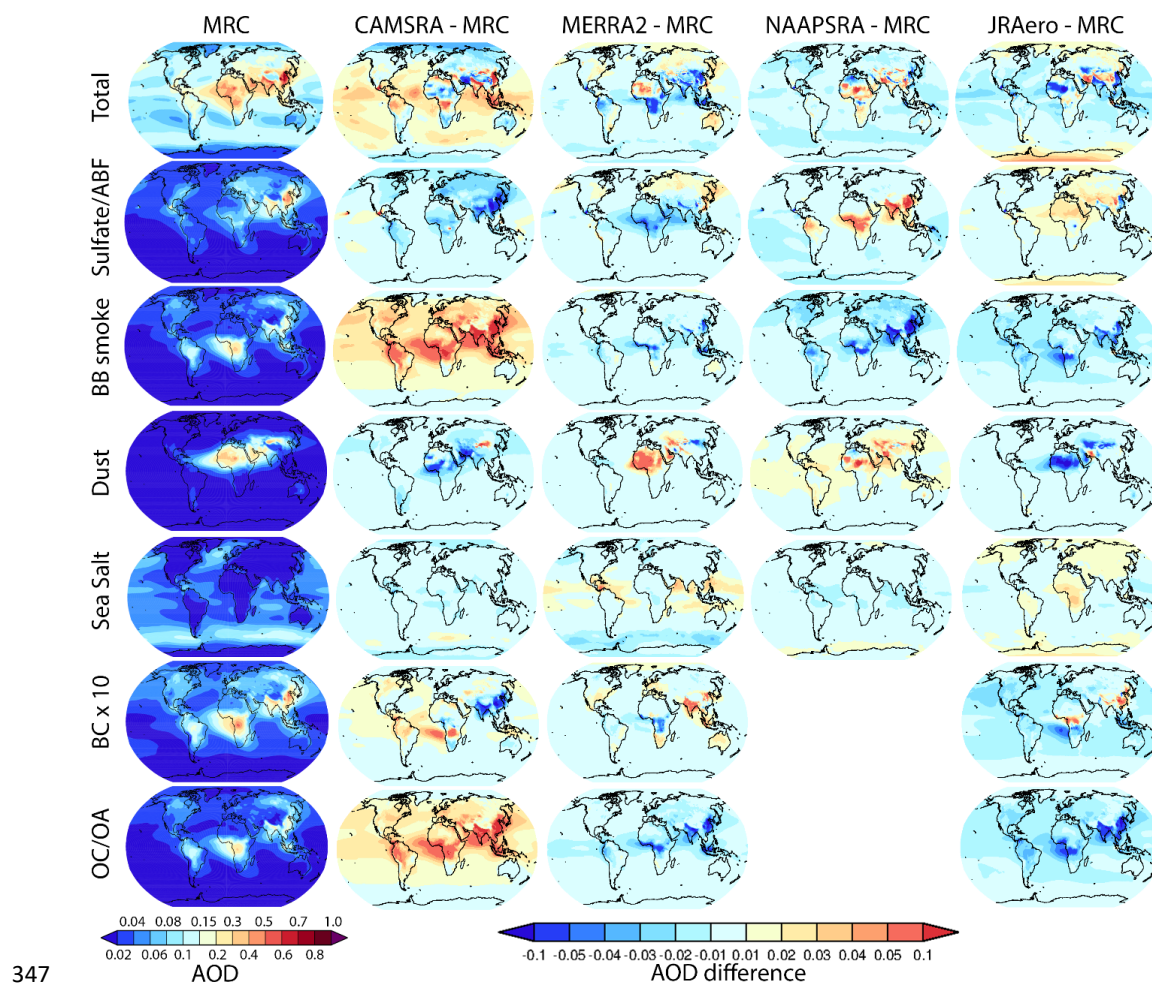
319

320 Figure 1. Annual and seasonal total 550nm AOD climatology from MODIS, the four RAs, and  
321 the MRC over 2003-2019, except JRAero for 2011-2019. The white area in MODIS plots means  
322 a lack of data.

323 The climatological annual and seasonal mean total AODs at 550nm from MODIS and the four  
324 aerosol RAs and their consensus (MRC) are presented in Figure 1. In general, there are very similar  
325 spatial AOD distribution patterns and AOD magnitude among the RAs and MODIS for all four  
326 seasons. This is expected as MODIS total AOD is assimilated into all of these products as well as  
327 used to tune the model components such as emissions. High AOD regions include the dust-  
328 dominated Sahara in Mar-Apr-May (MAM) and Jun-Jul-Aug (JJA), Sahel in Dec-Jan-Feb (DJF)  
329 and MAM, Southwest Asia and Taklamakan in MAM and JJA, anthropogenic pollution-  
330 dominated East Asia and South Asia throughout the year, BB smoke-dominated South Africa,  
331 South America in JJA and Sep-Oct-Nov (SON), Southeast Asia in MAM, Maritime Continent in  
332 SON, and high-latitude North America and Eurasia in JJA. For the annual mean, MODIS AOD is  
333 relatively high compared to the MRC in the northern hemisphere's high latitudes due to seasonal  
334 sampling bias. MODIS was able to retrieve AOD during biomass burning active season, i.e. boreal  
335 Summer-to-Fall, but it couldn't retrieve AOD during northern winter in the high latitudes due to  
336 the lack of sunlight. The high AOD over high-latitude Eurasia and North America in MODIS



337 annual mean is a general reflection of MODIS summertime AOD, which is captured by all the  
 338 RAs in their summertime mean AODs. It is also noted that all the RAs have slightly higher AOD  
 339 (on the order of 0.02) over the ocean than MODIS QAed product here. MODIS AOD products are  
 340 well known to low bias significant aerosol events (e.g., Reid et al., 2022; Gumber et al., 2023),  
 341 which could lower the mean state of AOD. The slightly lower MODIS AOD compared to the RAs  
 342 could also be related to clear-sky and contextual bias (Zhang et al., 2009), as MODIS AOD  
 343 retrieval is only available under clear-sky conditions, while all the RAs include all-sky conditions.  
 344 Sea salt and dust emissions are often associated with cloudy synoptic weather systems, and  
 345 hygroscopic aerosol species, such as sulfate, sea salt, and BB smoke, can potentially grow larger  
 346 in size in a moister environment, introducing a higher all-sky AOD than the clear-sky AOD.



347  
 348 Figure 2. Annual mean total and speciated AODs of the MRC and the AOD difference between  
 349 the individual RA and the MRC based on the 2011-2019 average.



350 Previous experience with multi-model ensembles suggests that the consensus of multi-models, in  
351 general, shows better skill than individual contributing models (Sessions et al., 2015; Xian et al.,  
352 2019; Reid et al., 2022). Similar verification conclusion is also drawn in Section 3.3. Therefore,  
353 the total and speciated AODs from the MRC based on the 2011-2019 average are used as a baseline  
354 here and are shown in Figure 2. As expected, sulfate/ABF AOD is relatively high over population-  
355 dense and industrially polluted regions, dust AOD is high over major desert and arid regions, and  
356 sea salt AOD is relatively high over mid-to-high latitude oceans. BB smoke and its components  
357 BC and OC/OA are relatively high over South Africa, South America, Southeast Asia, the  
358 Maritime continent, and Siberia, North American high latitudes major BB source regions. BC and  
359 OC/OA AOD are also relatively high over South Asia and East Asia, where sources other than  
360 BB, such as anthropogenic emission, are the main contributors, as suggested by contrasting smoke  
361 AOD contribution to the total AOD between NAAPS-RA and other RAs in these regions (Figures  
362 3 and 10. Noting that smoke AOD is driven by BB in NAAPS-RA, while smoke AOD is a sum  
363 of BC and OC/OA from the other RAs).

364 Shown also in Figure 2 are the total and speciated AOD differences between the individual RA  
365 and the MRC. For total AOD, CAMSRA is apparently higher than the other three RAs over the  
366 ocean, which is consistent with the findings on its operational counterpart of high biased FM AOD  
367 verified with Maritime Aerosol Network over the ocean in Reid et al. (2022). This high bias is  
368 attributed to its universally higher OA/smoke AOD compared to other RAs, and suggests that  
369 CAMSRA may have higher BB emissions and/or less efficient removals compared to the other  
370 RAs. Sulfate AOD is relatively low in CAMSRA except for some highly biased hotspots around  
371 outgassing volcanoes (in particular Mauna Loa and near Mexico City) as mentioned in Inness et  
372 al (2019). NAAPS-RA ABF AOD is higher than sulfate AOD in other RAs especially in East Asia,  
373 South Asia, central Africa, and north South America. This is expected as ABF in NAAPS-RA  
374 includes biogenic and anthropogenic primary and secondary aerosols besides sulfate. For dust  
375 AOD, MERRA-2 is relatively higher over north Africa and Arabian Peninsula and NAAPS-RA is  
376 relatively higher over most regions, including oceanic areas, while CAMSRA and JRAero are  
377 relatively lower over most regions except around Gobi desert for CAMSRA and Iran for JRAero.  
378 As for sea salt AOD, MERRA-2 is relatively higher over the tropical oceans, and lower over the  
379 southern ocean. JRAero sea salt AOD is relatively higher over most continents, which is probably  
380 unphysical.

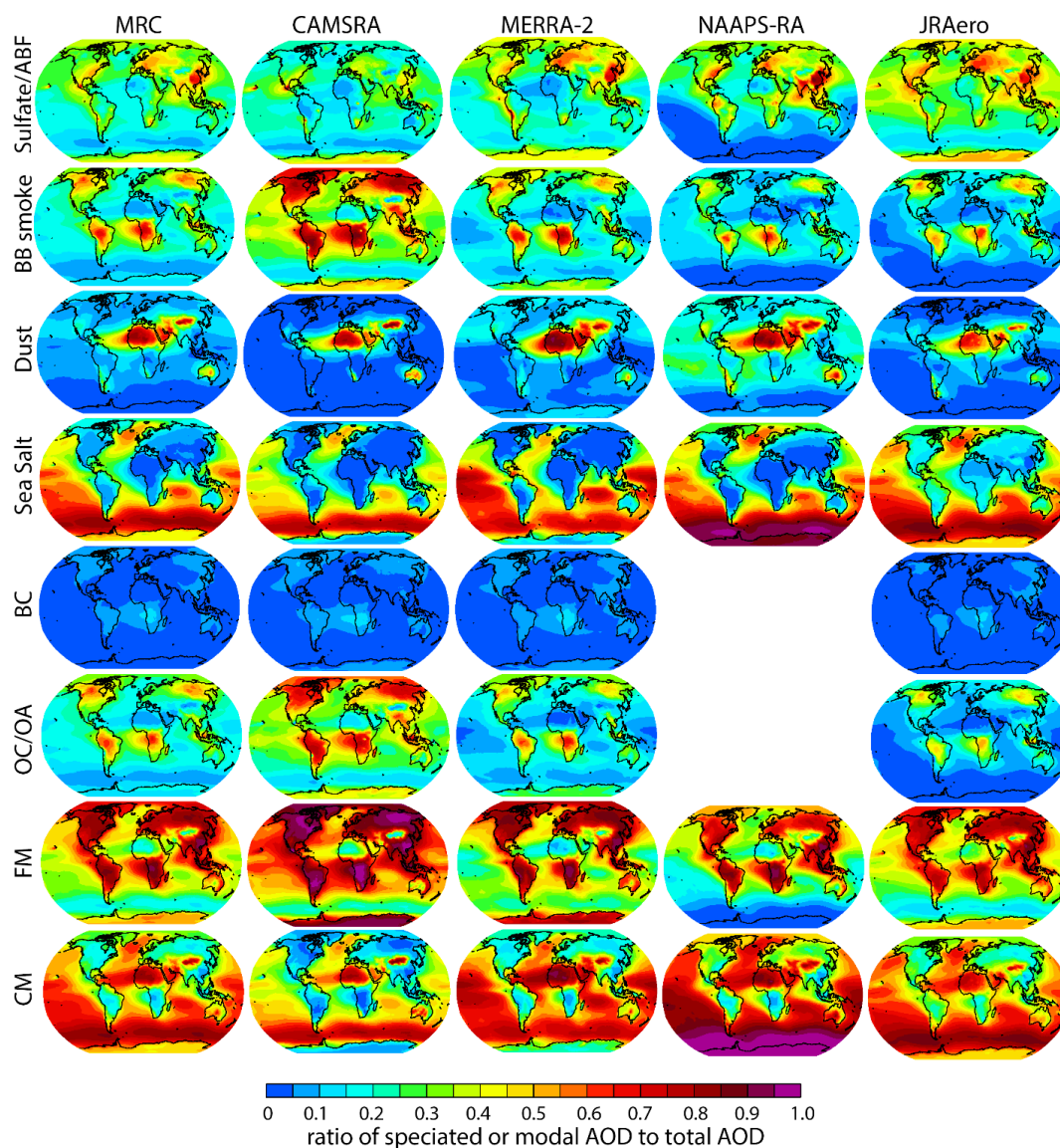
381 The differences in speciated AOD result in significant variations in their contributions to the total  
382 AOD, as illustrated in Figure 3. For instance, the considerably higher BB smoke AOD in  
383 CAMSRA compared to other RAs makes BB smoke the predominant contributor to total AOD in  
384 the CAMSRA over most continents, adjacent water bodies, and polar regions, except for regions  
385 where dust is dominant. Sulfate AOD, on the other hand, contributes more to the total AOD,  
386 particularly over oceanic regions in the JRAero compared to other RAs. Both MERRA-2 and  
387 JRAero exhibit higher sulfate contributions along the western coasts of South America and North  
388 America, suggesting possible increased production of dimethyl sulfide (DMS) in those areas. Dust  
389 AOD, on the other hand, contributes more to the total AOD particularly over oceanic regions in  
390 NAAPS-RA compared to the other RAs. Sea salt AOD is found to contribute more to the total



391 AOD in the high-latitude oceans and the Antarctic in NAAPS-RA compared to the other RAs. The  
392 OC/OA AOD contribution to the total AOD closely mirrors the distribution of BB smoke, as  
393 anticipated. The contribution of BC to the total AOD is generally small, ranging between 5-10%  
394 in BB regions, except for central South Africa where it reaches 10-15%. Despite the higher ratio  
395 of BB smoke AOD to total AOD ratio in CAMSRA, the ratio of BC to total AOD over East Asia  
396 and South Asia is smaller in CAMSRA compared to MERRA-2 and JRAero, suggesting that BC  
397 emissions from anthropogenic sources maybe lower in CAMSRA. Finally, the contributions of  
398 FM and CM AOD to the total AOD are also depicted in Figure 3. It is consistent among the RAs  
399 that FM is the dominant contributor over most land regions except for regions where dust is  
400 dominant, such as North Africa, the Arabian Peninsula, the Middle East, and the Gobi. In all the  
401 RAs, CM is the dominant contributor over oceanic regions, except for regions influenced by  
402 continental BB smoke and pollution outflow. The contribution of CM in CAMSRA is generally  
403 smaller in tropical to mid-latitude oceans compared to other RAs, due to its higher contribution  
404 from BB smoke. It is also noted that CM is dominant over FM in the Antarctic in NAAPS-RA,  
405 while FM is dominant in the Antarctic in the other three RAs, though total AOD is very small  
406 (annual and seasonal means  $< 0.04$  from MRC) and hard to validate due to lack of observational  
407 data.

408 Table 2 provides a summary of global-average total AOD and speciated AODs, as well as the  
409 contributions of speciated AOD to total AOD for all the RAs. Overall, the annual and global mean  
410 total AODs are similar, hovering around 0.14 for most RAs. However, CAMSRA stands out with  
411 a slightly higher total AOD of 0.151, which compared to the MRC is 0.012 higher, while the  
412 differences between the other RAs and MRC are within  $\pm 0.005$ . Total AODs over land show  
413 minimal variation among the RAs, likely due to the cancellation of high and low-biased speciated  
414 AODs. Over water, CAMSRA exhibits slightly higher AOD compared to other RAs.

415 Speciated AODs, especially smoke AOD and OA/OC AOD display greater diversity among the  
416 RAs. Smoke and OA AODs from CAMSRA are 2-3 times higher than those from the other RAs.  
417 Smoke AOD contributes to 41% of total AOD in CAMSRA, while ranging from 16%-22% in  
418 other RAs. Moreover, the standard deviation of smoke and OA AODs with respect to the 12  
419 months is also higher in CAMSRA than in other RAs. The contribution of dust AOD to total AOD  
420 varies from 13% to 28% for all the RAs, with NAAPS dust AOD being the highest among the RAs  
421 and about 2 times that of CAMSRA, which has the lowest dust AOD among the RAs. The  
422 contribution of sulfate/ABF AOD to total AOD ranges from 23% to 34%, with the highest  
423 contribution observed in JRAero. Sea salt AOD contributes 25% to 35% to total AOD in the RAs  
424 with JRAero being the highest. BC AOD, on the other hand, contributes only 3% to 4% of total  
425 AOD across the RAs. The FM's contribution to the overall AOD varies across different datasets.  
426 In MERRA-2, NAAPS-RA, and JRAero, FM accounts for 44% to 51% of the total AOD.  
427 However, in CAMSRA, its contribution is notably higher at 63%, primarily due to its significant  
428 contribution from BB. Conversely, CM's contribution to total AOD is consistent across the three  
429 RAs, ranging from 49% to 56%. In contrast, CM's contribution is lower, at 37%, in CAMSRA.



430

431 Figure 3. Ratio of speciated AODs, FM and CM AODs to total AOD from the MRC and the  
432 individual RAs based on the 2011-2019 annual average.

433 Table 2. Global area-weighted mean modal (total, FM, CM) and speciated AOD and standard  
434 deviation of monthly AOD based on 2011-2019 data. Percentage numbers in the brackets are  
435 contributions of speciated AOD to total AOD. Global mean total AODs over land and water are  
436 shown in the last two rows.



	global mean AOD					AOD standard deviation w.r.t. 12 months				
	CAMSRA	MERRA2	NAAPSRA	JRAero	MRC	CAMSRA	MERRA2	NAAPSRA	JRAero	MRC
total	0.151	0.137	0.134	0.134	0.139	0.018	0.010	0.011	0.012	0.013
dust	0.019 (13%)	0.029 (21%)	0.037 (28%)	0.021 (16%)	0.026 (19%)	0.008	0.009	0.009	0.009	0.008
sea salt	0.037 (25%)	0.041 (30%)	0.038 (28%)	0.045 (34%)	0.040 (29%)	0.001	0.001	0.003	0.002	0.001
sulfate/ABF	0.034 (23%)	0.037 (27%)	0.037 (28%)	0.046 (34%)	0.039 (28%)	0.002	0.001	0.001	0.002	0.001
smoke	0.062 (41%)	0.030 (22%)	0.022 (16%)	0.022 (16%)	0.034 (24%)	0.009	0.007	0.007	0.007	0.007
BC x 10	0.061 (4%)	0.059 (4%)		- 0.044 (3%)	0.054 (4%)	0.013	0.009		- 0.008	0.009
OC/OA	0.056 (37%)	0.024 (18%)		- 0.018 (13%)	0.033 (24%)	0.007	0.006		- 0.006	0.006
FM	0.096 (63%)	0.067 (49%)	0.059 (44%)	0.068 (51%)	0.073 (53%)					
CM	0.056 (37%)	0.070 (51%)	0.075 (56%)	0.066 (49%)	0.066 (47%)					
land total	0.180	0.174	0.175	0.176	0.176					
water total	0.136	0.118	0.112	0.111	0.112					

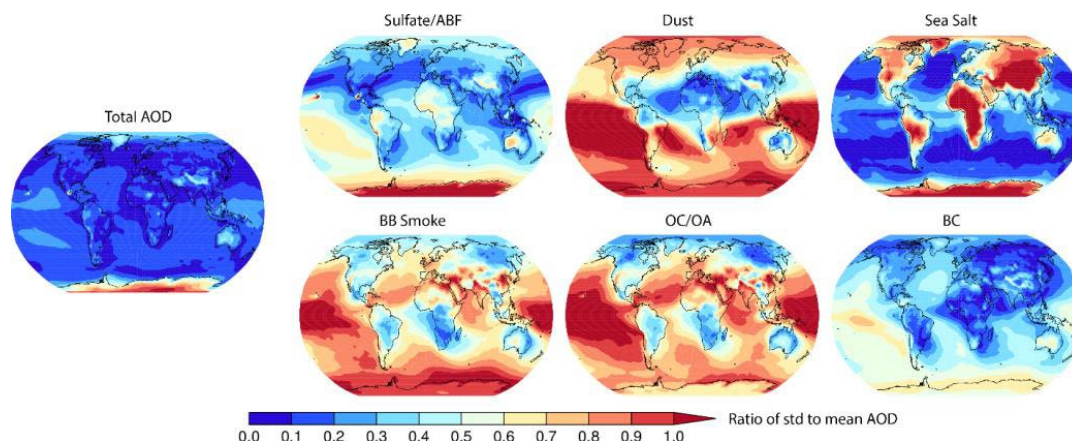
437

### 438 3.2 Geographical diversity of speciated AOD among the four reanalyses

439 The diversity of the global-average total and speciated AODs is already documented in Table 2.  
 440 Figure 4 provides the geographical distribution of the relative spread of speciated annual mean  
 441 AODs from the RAs to their means. Spread, in this context, is defined as the ratio of the standard  
 442 deviation of the RAs AODs to their mean. It is noteworthy that the relative spread of total AOD  
 443 from the four RAs is generally small, except for polar regions and specific hotspots where known  
 444 issues exist. For instance, biases in CAMSRA AOD have been identified over Hawaii and  
 445 Mexico's volcanic outgassing regions. In polar regions, there are limited satellite observations to  
 446 constrain model fields, resulting in a larger spread, which is consistent with the findings of Xian  
 447 et al. (2022) on AODs from CAMSRA, MERRA-2 and NAAPS-RA over the Arctic. Similarly,  
 448 over high terrains with snow and ice covers, such as the Himalayas and the Andes, and over desert  
 449 regions, such as the Australian deserts, and the Bodele Depression region in the Sahara, both  
 450 retrievals and models face challenges, leading to a larger spread. Moreover, over the Maritime  
 451 Continent, where high cloud coverage poses challenges to remote sensing retrievals for both AOD  
 452 and BB smoke emissions, the spread is also relatively large.

453 The aforementioned characteristics are also evident in the spread of speciated AODs. However,  
 454 the spreads of the speciated AODs among the RAs are much larger compared to the total AOD,  
 455 particularly in regions that are remote from aerosol sources. This suggests that the efficiency of  
 456 removal processes during long-range transport may differ. This is also relevant to the fact that data  
 457 assimilation constrains the total AOD, but speciated AOD remains unconstrained. Moreover, the  
 458 disparities in definitions of species, such as sulfate/ABF, BB smoke, OC/OA, as discussed in  
 459 Section 2.5, can also influence the spread of these FM species. The relative spread of speciated  
 460 AODs being much larger than that of total AOD, is broadly consistent with the AeroCom results,  
 461 where global climate models (without data assimilation) were intercompared in terms of aerosol  
 462 optical properties and life cycles (Kinne et al., 2006; Textor et al., 2006; Gliš et al., 2021).

463



464

465 Figure 4. Spread of total and speciated climatological annual-mean AOD among the four RAs.  
466 Spread here is defined as the ratio of the standard deviation of the RA AODs to their mean.

### 467 3.3. Evaluation with AERONET AOD

468 This section presents evaluation of the monthly performance of the four RAs plus the consensus  
469 at the AERONET sites on regional and global scales. Both skill and consistency of the different  
470 RAs and consensus are evaluated.

#### 471 3.3.1 Bias, RMSE, and correlation between the RAs and AERONET

472

473 The regional and global mean modal AOD bias, RMSE, and square of the correlations for the four  
474 RAs and the MRC are shown as bar graphs on global maps in Figures 5, 6 and 7. Regarding  
475 regional bias, all the RAs except for CAMSRA, have large negative biases (on the order of -0.1)  
476 in total AOD over Southeast Asia, South Asia, and the Maritime continent (Figure 5). The much  
477 smaller negative bias in total AOD over these regions in CAMSRA is a result of the cancellation  
478 of a positive bias in FM, possibly due to high biased OA/smoke AOD, and a negative bias in CM.  
479 The large negative biases over these regions in the other RAs are mainly attributed to large negative  
480 biases in FM AOD in general. It is also noted that CAMSRA is biased relatively high in total AOD  
481 due to high FM bias over East Asia. Over other regions and the globe, all the RAs have relatively  
482 small biases and in general slight positive biases, with CAMSRA having the largest positive bias,  
483 due mainly to relatively high OA/smoke AOD. The cancellation effect of positive FM bias and  
484 negative CM bias in CAMSRA are also visible.

485

486 Total AOD RMSEs are relatively high over all Asian regions and North Africa compared to other  
487 regions for all the RAs (Figure 6). The contribution of FM to total AOD RMSE is larger than that  
488 from CM globally, except over dust-influenced regions, including North Africa and, for most  
489 models, Southwest Asia and Central America. The correlations of total AOD between the RAs and  
490 AERONET data are mostly reasonable for all the regions (Figure 7). Some relatively low-  
491 performance regions (total AOD  $r^2$  less than 0.60 for at least one RA) include South Asia,  
492 Southwest Asia, Australia, Europe, and East Asia. The relatively low correlations over Australia  
493 and Europe are due to the low climatological mean and variance. While the other low-performance



494 regions are all mixed pollution and dust environment that is challenging for all RAs. Some  
495 relatively high-performance regions (total AOD  $r^2$  greater than 0.90 for at least two RA members)  
496 include Central America, Peninsula Southeast Asia, and Maritime Continent. Total and CM AOD  
497  $r^2$  are high over Central America, because it is a receptor region for African dust, and RAs perform  
498 well in general during long-range transport over ocean where data assimilation is very effective in  
499 correcting model AOD fields. Total and FM AOD  $r^2$  are high over Peninsula Southeast Asia, and  
500 Maritime Continent, because the regional dominant aerosol species, BB smoke, have large  
501 interannual variabilities, due to the impact of ENSO on fire activities in the regions (e.g., Reid et  
502 al., 2012; Xian, et al., 2013). Overall, the MRC exhibits superior  $r^2$  compared to individual RAs  
503 for modal AODs regionally and globally.

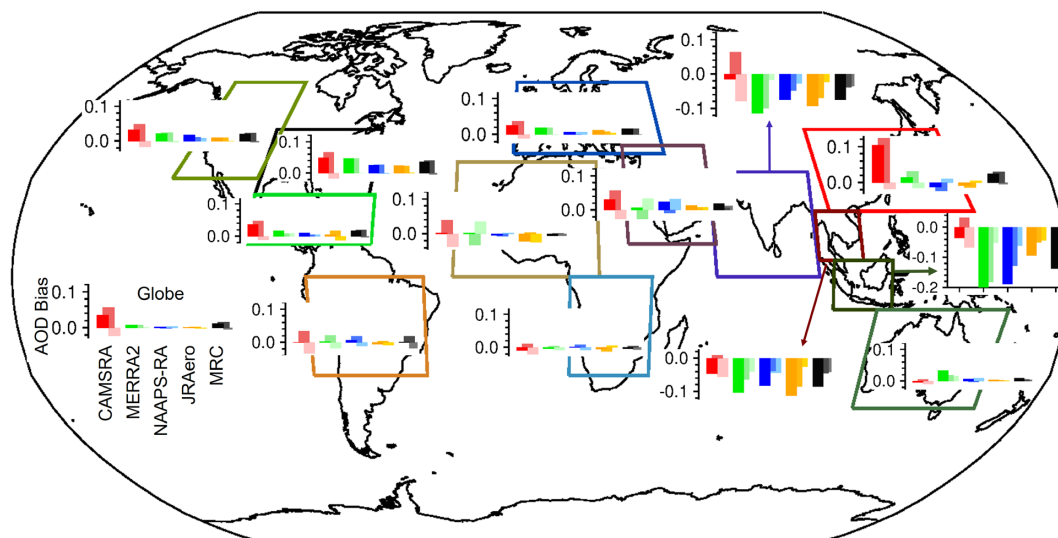
504

505 For remote marine sites, including Ascension Island in the mid-basin of south Atlantic, Ragged  
506 Point in the western Tropical Atlantic, Mauna Loa in Hawaii, MCO-Hanimaadhoo in the north  
507 Indian Ocean, and REUNION\_DENIS in the south Indian Ocean, the RAs exhibit similar  
508 performance at these sites as they do over the upwind land or coastal regions (Fig. S1). An  
509 exception is Maura Loa. Maura Loa is situated at an elevation of 3.4 km, well above the marine  
510 boundary layer and remote from continental sources. At this location, all the RAs exhibit a  
511 significant positive bias. One possible explanation for this bias is the topographic effect, as the  
512 coarse spatial resolutions of the models may not be able to resolve the site's high elevation.  
513 Additionally, uncertainties in the removal processes during long-range transport may also be  
514 contributing to the high bias.

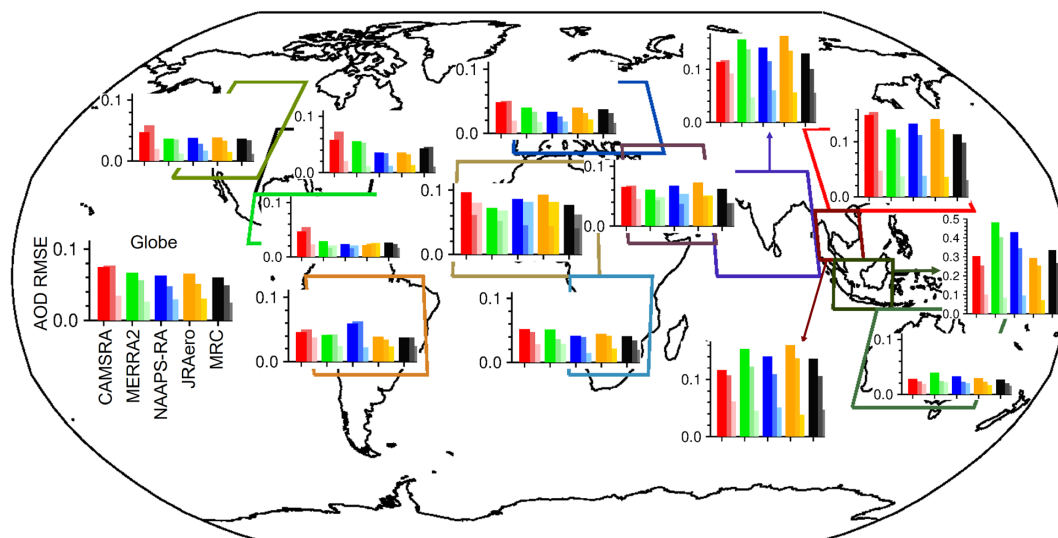
515

516 When considering the contribution of dust and sea salt aerosols to FM AOD in CAMSRA,  
517 MERRA-2 and JRAero, the verification statistics (bias, RMSE and  $r^2$ ) for the total AOD of these  
518 RAs remain unchanged as expected (Fig. S2, S3, S4). However, there is a noticeable shift in the  
519 positive bias of FM AOD (and negative bias of CM AOD) for these RAs, particularly in regions  
520 influenced by dust, such as North Africa, the Arabian Peninsula, East Asia, Central America, South  
521 Asia, and Europe. Specifically, the positive bias in FM AOD becomes more pronounced, and the  
522 negative bias in CM AOD becomes more negative in these regions, especially for CAMSRA. It's  
523 worth noting that in MERRA-2, there is a change in sign, where the FM AOD bias switches from  
524 negative to positive in North Africa and the Arabian Peninsula, while the CM AOD bias changes  
525 from positive to negative in these regions. Additionally, the negative FM AOD bias becomes  
526 smaller, however the negative CM AOD bias worsens in South Asia within both MERRA-2 and  
527 JRAero datasets (Fig. S2). In general, when taking into account the contribution of dust and sea  
528 salt aerosols to FM AOD (by default, dust and sea salt AODs are treated as CM AODs in this  
529 study) in CAMSRA, MERRA-2, and JRAero, we observe a worsening of both FM and CM AOD  
530 biases in these three datasets. Similarly, the RMSE for both FM and CM AODs over regions  
531 influenced by dust deteriorates as well (Fig. S3). The  $r^2$  for FM and CM AODs in these regions  
532 also worsens overall, with the exception of an improvement in FM AOD over Central America.  
533 FM sea salt's impact on the verification score is small as the majority of AERONET sites are on  
534 land and FM sea salt only contributes on the order of ~10% to total sea salt AOD in the three RAs.

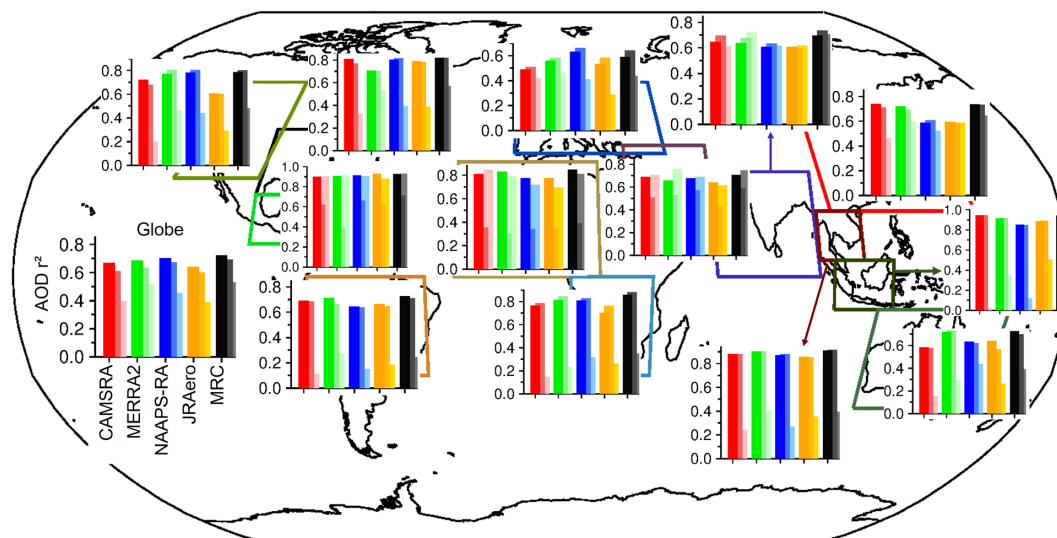
535



536  
537 Figure 5. Regional total, FM, and CM AOD biases for the four reanalyses and the MRC  
538 compared with AERONET data. Each grouped bars in the same color system present total, FM,  
539 and CM AOD biases from left to right (also dark to light).  
540  
541



542  
543 Figure 6. Same as Figure 5, except for AOD RMSE.



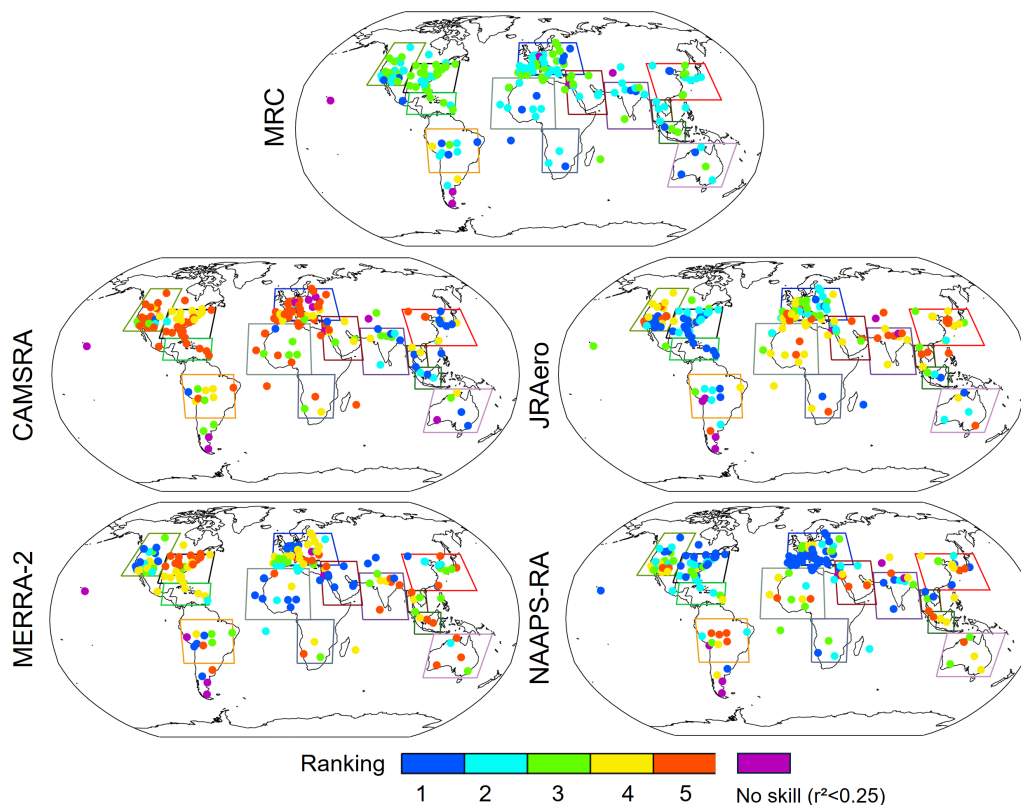
544  
545 Figure 7. Same as Figure 5, except for the AOD coefficient of determination ( $r^2$ ).  
546

547  
548 3.3.2 Rankings of the RAs with respect to validation statistics

549 To expand the validation result from regional averages to individual sites, including remote sites  
550 that are not included in the regional analysis, rankings of the RAs in terms of RMSE of monthly  
551 total AOD at all the AERONET sites are displayed in Figure 8. It shows that there are cases in that  
552 individual RA ranks first over some regions. For example, CAM5RA ranks relatively better than  
553 others in South and Southeast Asia, MERRA2 ranks better over North Africa and Arabia  
554 Peninsula, NAAPS-RA ranks better over North America and Europe while JRAero performs  
555 relatively better over Southern North America and the Caribbean. Individual reanalysis has mixed  
556 results for sites in other regions. AOD RMSE of the MRC is not always the lowest for a given site,  
557 but it is relatively low and stable over the globe. This is consistent with the regional RMSE result  
558 (Figure 6). The consensus wins because of its averaging of independent models. This is consistent  
559 with our findings with the ICAP models.

560  
561 Challenging sites for these RAs are found as marked by the magenta color in Figure 8. These sites  
562 exhibit an  $r^2$  value of less than 0.25, and are associated with relatively large AOD bias and/or  
563 RMSE. Often, when a challenge occurs, it is a common challenge to all models, and no specific  
564 model is much better than the others. Some of the causes for the challenges include lack or large  
565 uncertainty in local emissions (e.g. Modena in Northern Italy, Mainz in Germany, Cario\_EMA in  
566 Egypt, Trelew and CEILAP-RG sites in Argentina), and/or topographic effects that are not  
567 resolved in these RAs due mostly to coarse model spatial resolutions (e.g., Mauna\_Loa), and sites  
568 that are impacted by mixed pollution and dust (Dushanbe in Tajikistan).

569



570

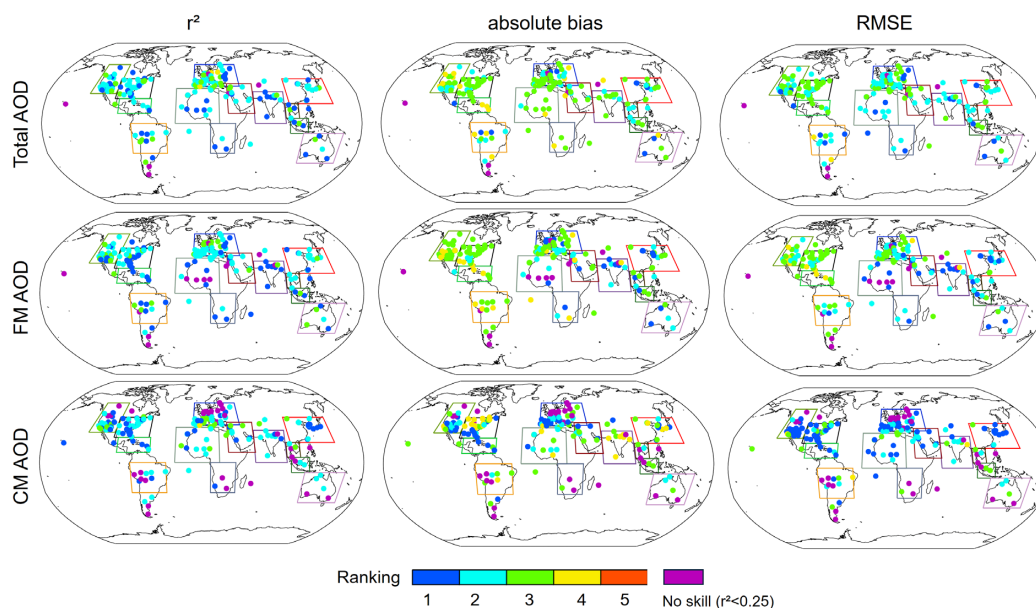
571 Figure 8: Ranking of aerosol RAs in terms of RMSE of monthly total AOD at 550nm over all the  
572 AERONET sites. Rectangles are used to delineate regions for regional validation, as depicted in  
573 Figures 5, 6, 7. A lower RMSE indicates better performance, with a ranking of 1 being the most  
574 desirable. AERONET sites with a coefficient of determination ( $r^2$ ) less than 0.25 are marked in  
575 magenta, indicating a lack of skill from the model.

576

577 Ranking analyses were also conducted on the RMSEs of FM and CM AODs, absolute bias, and  
578 coefficient of determination ( $r^2$ ) of modal AODs. Figure 9 presents the MRC rankings for all these  
579 comparison statistics. In line with the MRC ranking for the total AOD's RMSE, the MRC rankings  
580 for other metrics are predominantly ranked first or second, except for the absolute biases, where  
581 MRC rankings are often ranked third over North America and Europe for total and FM AODs. For  
582 these modes and over these regions, all the RAs have positive biases relative to AERONET. When  
583 the biases are in the same sign (positive or negative), it is mathematically natural for MRC to rank  
584 in the middle. For CM and FM AODs, there are more sites with  $r^2 < 0.25$  compared to the total  
585 AOD. These sites mostly have small values of CM or FM AODs, and reside in regions of opposite-  
586 mode dominance, such as FM in Saharan region, CM in northern Europe and N. America. From  
587 another perspective, the MRC ranking with respect to correlations is superior to RMSE and then  
588 absolute bias. That is, the MRC better captures aerosol variance than the individual models, but is  
589 nevertheless subject to overall model biases. The MRC ranking for CM AOD is slightly superior  
590 to that of total AOD and then FM AOD. While the MRC ranking is not consistently at the top for



591 a given site or region, it is relatively high and stable, ranking first for the global average. No  
592 individual RAs could compete with the MRC in that sense.



593  
594 Figure 9. Ranking of the MRC among all the RAs in terms of  $r^2$ , absolute bias, and RMSE of the  
595 total, FM, and CM AODs over AERONET sites.

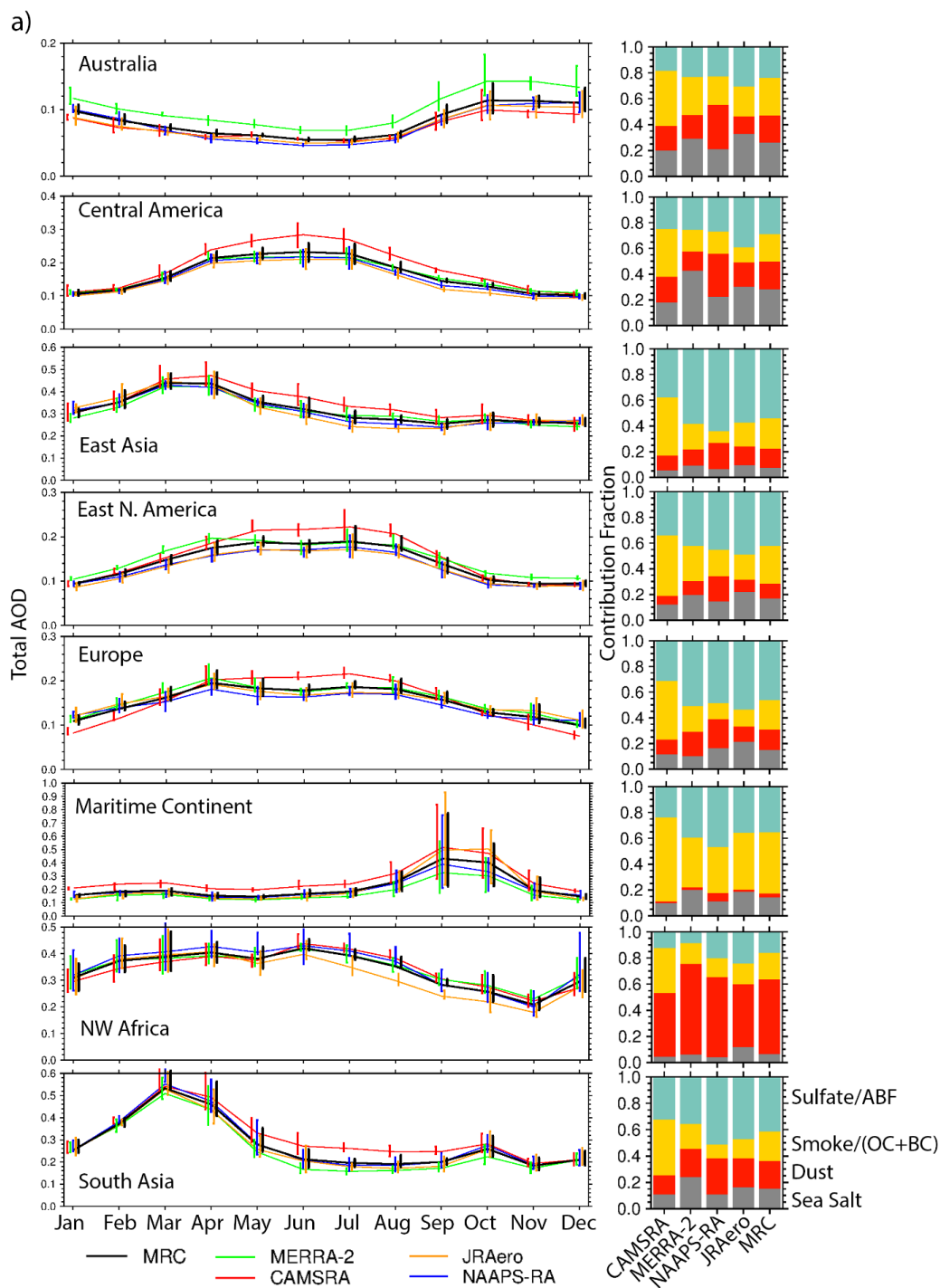
### 596 597 3.4 Seasonality of Regional AODs

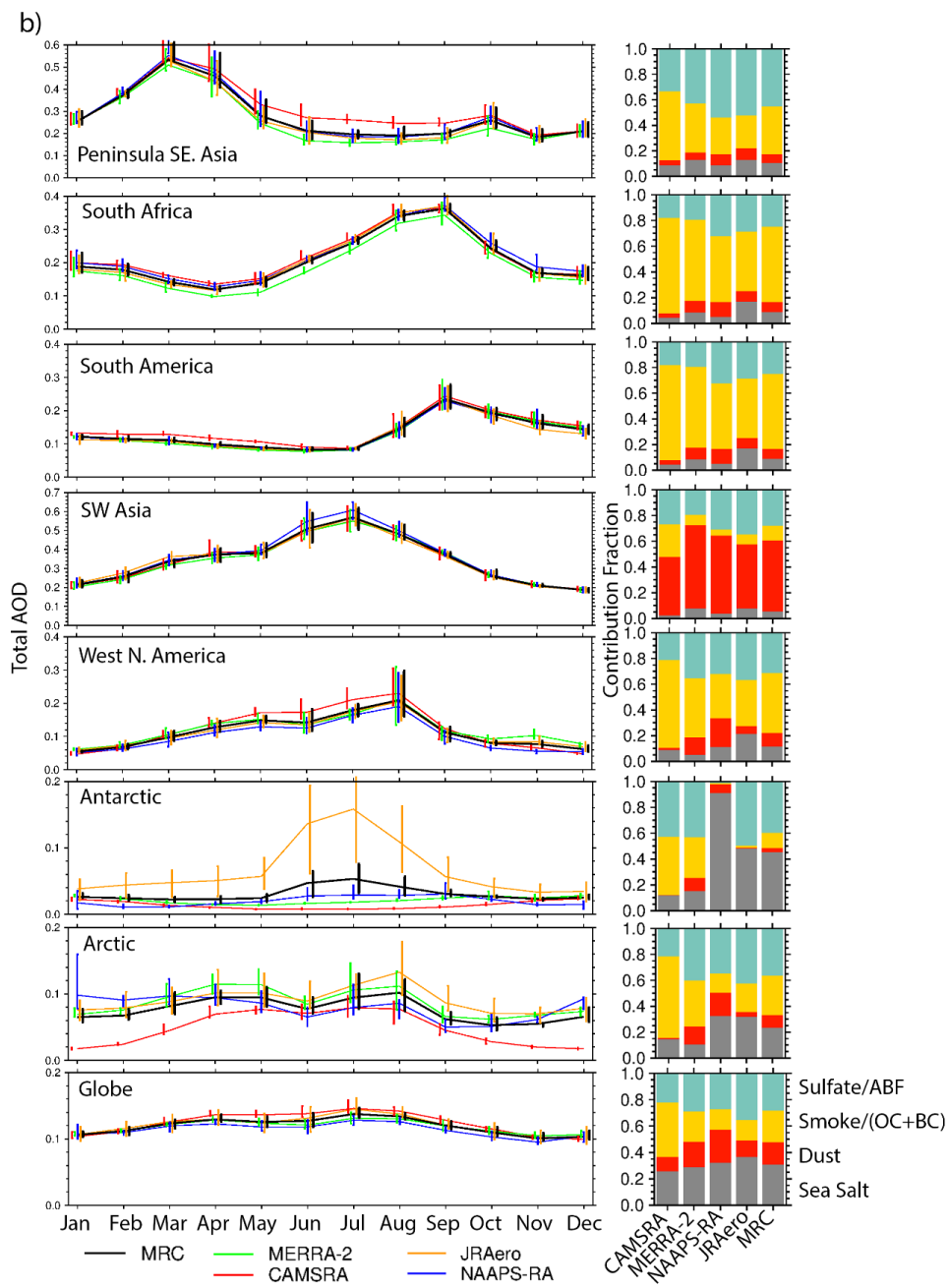
598 In Section 3.1 we depict the spatial distribution of total AODs from all the RAs across the four  
599 seasons. In this section, we provide monthly time series of AOD and AOD interannual variabilities  
600 for 16 regions (Fig. 10), along with the contributions of speciated AOD to the total AOD for these  
601 regions. All the RAs exhibit a similar seasonality and interannual variability of total AOD for all  
602 regions, except for the Antarctic and Arctic, particularly during their winter seasons. This disparity  
603 arises from the absence of passive satellite AOD data during polar winter, which limits the effect  
604 of data assimilation on model AOD (Xian et al., 2022). Even during polar summer, AOD retrievals  
605 are often unavailable due to high reflectance from surface ice/snow. The polar regions demonstrate  
606 the most significant diversity among the RAs in the seasonal cycle and speciation of AOD.

607  
608 The regions that are dominated by BB-smoke, including South Africa, South America, Maritime  
609 Continent, Peninsula SE Asia, and western North America, exhibit consistent peak seasons of total  
610 AOD with their respective burning seasons. The Maritime Continent and Peninsula SE Asia  
611 experience extremely large interannual variations of peak monthly AOD, owing to a strong  
612 positive correlation between burning activities and El Nino cycles (e.g., Reid et al., 2012; Xian et  
613 al., 2013). The contributions of sulfate/ABF AOD induced by pollution are dominant in East Asia  
614 and South Asia, while other aerosol species also make a significant contribution to the total AOD.  
615 In Europe and East N. America, sulfate/ABF is also the dominant species; however, the monthly  
616 total AOD values are much smaller. All the RAs capture the dominance of dust species in  
617 summertime over SW Asia and NW Africa. The relatively high AOD in springtime in NW Africa  
618 is partially due to BB in Sahel. In Australia, the peak AOD in Oct-Dec is associated with BB



619 smoke. In Central America, the relatively high AOD in the springtime results from BB smoke.  
620 Although quite diverse in AOD magnitude, all RAs tend to have a summertime total AOD peak  
621 attributed to dust. For the global average, sea salt AOD has a significant contribution to the total  
622 AOD as the area of the ocean overwhelms the area of land. Monthly time series of the speciated  
623 AODs for all the regions are available in the Figure S5. Overall, the seasonality and interannual  
624 variability of total AOD for most regions is very similar among the RAs. Moreover, all RAs have  
625 the same dominant species for most regions, but the contributions from different species can be  
626 quite different in these RAs. This is a result of the fact that total AOD is constrained within these  
627 RAs through data assimilation, while speciated AODs are not. Aerosol speciation and the  
628 contribution of each species to the total AOD are determined by the construction of the aerosol  
629 forecast models, which are very independent in these RAs.  
630







633

634 Figure 10. Climatological seasonal cycle of regional mean total AOD (left), and contribution  
635 fraction of speciated AOD to the total AOD for the corresponding regions from the four RAs and  
636 the MRC (right). Bars in the seasonal cycle plots represent the interquartile range of monthly-  
637 mean AOD for 2011-2019.

638

#### 639 4. Conclusions

640 This study compares the monthly average total, and speciated aerosol optical depths (AODs) from  
641 four different aerosol reanalyses (RAs). These include the Copernicus Atmosphere Monitoring  
642 Service ReAnalysis (CAMSRA) developed by Copernicus/ECMWF; the Japanese Reanalysis for  
643 Aerosol (JRAero) developed at the Japan Meteorological Agency (JMA); the Modern-Era  
644 Retrospective Analysis for Research and Applications, version 2 (MERRA-2) developed by  
645 NASA; and the Navy Aerosol Analysis and Prediction System reanalysis (NAAPS-RA),  
646 developed by the U.S. Naval Research Laboratory. The consensus of the four RAs is also  
647 developed for intercomparison. The AODs from these RAs are evaluated with AEROSol Robotic  
648 NETWORK (AERONET) and the combined MODIS Dark Target/Deep Blue retrievals (Levy et al.,  
649 2013; Sayer et al. (2014)) using data from 2011-2019. The following are the conclusions drawn  
650 from this study:

651 1) Global distribution and magnitude of total AOD demonstrate a high level of similarity  
652 among all four RAs. The spread of total AOD among the RAs is small over most regions.  
653 Exceptions, where the RAs diverge in total AOD are polar regions and areas affected by  
654 specific factors, including volcanic outgassing, high terrains, and certain desert regions.

655 2) The relative spread of speciated AODs is considerably larger than that of total AOD.  
656 CAMSRA consistently yields higher values for biomass burning (BB) smoke or Organic  
657 Aerosol (OA) AOD in comparison to other RAs. Meanwhile, NAAPS-RA exhibits  
658 generally higher dust AOD values. JRAero has comparatively high biased inland sea salt  
659 AOD. The diversity of speciated AODs in regions remote from aerosol sources is large,  
660 implying different efficiencies in removal during long-range transport. This phenomenon  
661 results from the fact that data assimilation in these RAs constrains total AOD but not  
662 speciated AOD.

663 3) The seasonality and interannual variability of total AOD in the 16 regions under study,  
664 with the exception of the Antarctic and Arctic, demonstrate a high degree of similarity  
665 across the various RAs. While the dominant species of aerosols are consistent across most  
666 regions in all RAs, the relative contributions from individual species can vary significantly.

667 4) The accuracy of the RAs, as measured by RMSE, bias, and correlation of the total, fine-  
668 mode (FM) and coarse-mode (CM) AODs, has been verified with AERONET. It is evident  
669 that each RA exhibits its own unique regional strengths. Specifically, CAMSRA performs  
670 better in South and Southeast Asia, MERRA-2 excels in African and Arabian Peninsula  
671 dust regions, NAAPS-RA shows relatively better performance over Europe and East  
672 CONUS, and JRAero performs relatively better over southern North America and the  
673 Caribbean. Common challenges to all the RAs often include lack or large uncertainty in



674 local emissions, and/or topographic effects, as well as situations where both FM and CM  
675 states are mixed. RAs show the worst performance in areas impacted by mixed FM and  
676 CM aerosols, such as South Asia and East Asia, and areas that experience substantial  
677 interannual variability in AOD, for instance, Southeast Asia, and the Maritime Continent.  
678 The polar regions present a challenge due to limited observations.

679 5) The Multi-Reanalysis-Consensus (MRC), based on the four RAs, is not consistently the  
680 best performer in terms of RMSE, bias and correlation of modal AODs for a given site or  
681 region. However, the MRC generally performs relatively well and remains stable, ranking  
682 first or second regionally and first globally among all the RAs, especially for correlation  
683 and RMSE. The MRC ranking with respect to correlations is superior to RMSE and then  
684 absolute bias. The MRC ranking for CM AOD is slightly superior to that of total AOD and  
685 then FM AOD. The MRC method gains an advantage due to its ability to average  
686 independent models.

687 The findings presented in this study offer a comprehensive overview of the current state-of-the-art  
688 aerosol reanalyses in the context of monthly AOD. The strengths and weaknesses of individual  
689 reanalyses and their collective implications will provide valuable information for diverse potential  
690 users. Compared to intercomparisons of satellite AOD products, which have shown a typical bias  
691 of 15%-25% (which regionally can reach  $\pm 50\%$ ) and AOD diversity of 10% over ocean to 100%  
692 over certain land areas amongst 14 satellite products (Schutgens et al., 2020), the biases and  
693 diversity of AODs from the four reanalyses are moderate.

694 The results of the intercomparison highlight areas for improvement in the next generation of  
695 aerosol reanalyses. These improvements may include tuning of emission sources and sinks, finer  
696 spatiotemporal resolutions, incorporation of additional aerosol species, such as nitrate aerosols and  
697 dust with different mineralogy, separation of BC and OC from BB emissions in some RAs, and  
698 application and enhancement of BB plume rise models. Moreover, some centers are planning to  
699 incorporate new observational data, such as OMI Aerosol Index to constrain the amount of  
700 absorptive aerosols, which has the potential to enhance simulations of BB smoke and dust aerosols  
701 (Zhang et al., 2021, Sorenson et al, 2023). Anticipated advancements in emission inventories,  
702 retrieval algorithms, space-borne sensors, upcoming satellite missions, and improvements in  
703 meteorological and aerosol modelling are expected to drive progress in aerosol reanalyses.

704

705

#### 706 **Data Availability**

707 All the data supporting the findings of this manuscript can be accessed via the provided links or  
708 by requesting them using the contact information provided within those links.

709 AERONET Version 3 Level 2 data: <http://aeronet.gsfc.nasa.gov>

710 MODIS data-assimilation-quality AOD:

711 <https://modaps.modaps.eosdis.nasa.gov/services/about/products/c61-nrt/MCDAODHD.html>



712 CAMSRA AOD: <https://www.ecmwf.int/en/research/climate-reanalysis/cams-reanalysis>

713 JRAero product: <https://www.riam.kyushu-u.ac.jp/taikai/JRAero/>

714 MERRA-2 AOD:

715 [https://disc.gsfc.nasa.gov/datasets/M2TMNXAER\\_V5.12.4/summary?keywords=%22MERRA-](https://disc.gsfc.nasa.gov/datasets/M2TMNXAER_V5.12.4/summary?keywords=%22MERRA-2%22)  
716 [2%22](https://disc.gsfc.nasa.gov/datasets/M2TMNXAER_V5.12.4/summary?keywords=%22MERRA-2%22)

717 NAAPS RA AOD: [https://usgodae.org/cgi-](https://usgodae.org/cgi-bin/datalist.pl?dset=nrl_naaps_reanalysis&summary=Go)

718 [bin/datalist.pl?dset=nrl\\_naaps\\_reanalysis&summary=Go](https://usgodae.org/cgi-bin/datalist.pl?dset=nrl_naaps_reanalysis&summary=Go)

719

## 720 **Supplement**

721

## 722 **Author contributions**

723 PX and JSR designed the study. PX performed the data analysis and wrote the paper with  
724 contributions from MA, PRC, KY, TFE, EJH on data descriptions. All authors contributed to the  
725 discussion of the results and revising the paper.

## 726 **Competing interests**

727 The contact author has declared that none of the authors has any competing interests.

## 728 **Acknowledgments**

729 The authors acknowledge financial supports from the Office of Naval Research Code 322. Partial  
730 support comes from NASA's Interdisciplinary Science (IDS) program (grant no.  
731 80NSSC20K1260). We also thank the NASA AERONET and MODIS teams for the AOD data  
732 used in the study. We extend our gratitude to NASA GMAO, ECMWF, JMA, U.S. ONR and NRL  
733 for providing access to the aerosol reanalysis products.

## 734 **References**

735 Atwood, S. A., Reid, J. S., Kreidenweis, S. M., Blake, D. R., Jonsson, H. H., Lagrosas, N. D.,  
736 Xian, P., Reid, E. A., Sessions, W. R., and Simpas, J. B.: Size-resolved aerosol and cloud  
737 condensation nuclei (CCN) properties in the remote marine South China Sea – Part 1:  
738 Observations and source classification, *Atmos. Chem. Phys.*, 17, 1105–1123,  
739 <https://doi.org/10.5194/acp-17-1105-2017>, 2017.

740 Buchard, V., Silva, A. M. da, Colarco, P. R., Darmenov, A., Randles, C. A., Govindaraju, R.,  
741 Torres, O., Campbell, J., and Spurr, R. (2015) Using the OMI aerosol index and absorption  
742 aerosol optical depth to evaluate the NASA MERRA Aerosol Reanalysis, *Atmos Chem Phys*, 15,  
743 5743–5760, <https://doi.org/10.5194/acp-15-5743-2015>.

744

745 Buchard, V., Randles, C. A., Silva, A. M. da, Darmenov, A., Colarco, P. R., Govindaraju, R.,  
746 Ferrare, R., Hair, J., Beyersdorf, A. J., Ziemba, L. D., and Yu, H. (2017) The MERRA-2 Aerosol



- 747 Reanalysis, 1980 Onward. Part II: Evaluation and Case Studies, *J Climate*,  
748 <https://doi.org/10.1175/jcli-d-16-0613.1>.  
749
- 750 Colarco, P. R., Kahn, R. A., Remer, L. A., and Levy, R. C. : Impact of satellite viewing-swath  
751 width on global and regional aerosol optical thickness statistics and trends. *Atmospheric*  
752 *Measurement Techniques*, 7, 2313–2335, 2014.
- 753 Cui, C.; Liu, Y.; Chen, L.; Liang, S.; Shan, M.; Zhao, J.; Liu, Y.; Yu, S.; Sun, Y.; Mao, J.;  
754 Zhang, H.; Gao, S.; Zhenxing Ma, Z (2022) Assessing public health and economic loss  
755 associated with black carbon exposure using monitoring and MERRA-2 data, *Environmental*  
756 *Pollution*. 313, 120190, ISSN 0269-7491, doi: <https://doi.org/10.1016/j.envpol.2022.120190>.
- 757 Dee, D. P., and A. M. da Silva (1999) Maximum-likelihood estimation of forecast and  
758 observation error covariance parameters. Part I: Methodology. *Mon. Wea. Rev.*, 127, 1811–  
759 1834, doi:10.1175/1520-0493(1999)127<1822:MLEOFA.2.0.CO;2.  
760
- 761 Dee, D., L. Rukhovets, R. Todling, A. M. da Silva, and J. W. Lawson (2001) An adaptive buddy  
762 check for observational quality control. *Quart. J. Roy. Meteor. Soc.*, 127, 2451–2471,  
763 doi:10.1002/qj.49712757714.  
764
- 765 Diehl, T., A. Heil, M. Chin, X. Pan, D. Streets, M. Schultz, and S. Kinne (2012) Anthropogenic,  
766 biomass burning, and volcanic emissions of black carbon, organic carbon, and SO<sub>2</sub> from 1980 to  
767 2010 for hindcast model experiments. *Atmos. Chem. Phys. Discuss.*, 12, 24 895–24 954,  
768 doi:10.5194/acpd-12-24895-2012.  
769
- 770 Eck, T.F., Holben, B.N., Reid, J.S., Dubovik, O., Smirnov, A., O’Neill, N.T., Slutsker, I., Kinne,  
771 S., 1999. Wavelength dependence of the optical depth of biomass burning, urban, and desert dust  
772 aerosols. *J. Geophys. Res.* 104 (D24), 31,333–31,349.
- 773 Eck, T. F., Holben, B. N., Reid, J. S., Xian, P., Giles, D. M., Sinyuk, A., et al.  
774 (2018). Observations of the interaction and transport of fine mode aerosols with cloud and/or  
775 fog in Northeast Asia from Aerosol Robotic Network and satellite remote sensing. *Journal of*  
776 *Geophysical Research: Atmospheres*, 123, 5560– 5587. <https://doi.org/10.1029/2018JD028313>
- 777 Edwards, E.-L., Reid, J. S., Xian, P., Burton, S. P., Cook, A. L., Crosbie, E. C., Fenn, M. A.,  
778 Ferrare, R. A., Freeman, S. W., Hair, J. W., Harper, D. B., Hostetler, C. A., Robinson, C. E.,  
779 Scarino, A. J., Shook, M. A., Sokolowsky, G. A., van den Heever, S. C., Winstead, E. L.,  
780 Woods, S., Ziemba, L. D., and Sorooshian, A.: Assessment of NAAPS-RA performance in  
781 Maritime Southeast Asia during CAMP<sup>2</sup>Ex, *Atmos. Chem. Phys.*, 22, 12961–12983,  
782 <https://doi.org/10.5194/acp-22-12961-2022>, 2022.  
783
- 784 Flemming, J., Benedetti, A., Inness, A., Engelen, R. J., Jones, L., Huijnen, V., Remy, S.,  
785 Parrington, M., Suttie, M., Bozzo, A., Peuch, V.-H., Akritidis, D., and Katragkou, E.: The  
786 CAMS interim Reanalysis of Carbon Monoxide, Ozone and Aerosol for 2003–2015, *Atmos.*  
787 *Chem. Phys.*, 17, 1945–1983, <https://doi.org/10.5194/acp-17-1945-2017>, 2017.  
788



- 789 Gelaro, R., McCarty, W., Suarez, M. J., Todling, R., Molod, A., Takacs, L., Randles, C. A.,  
790 Darnenoy, A., Bosilovich, M. G., Reichle, R., Wargan, K., Coy, L., Cullather, R., Draper, C.,  
791 Akella, S., Buchard, V., Conaty, A., Silva, A. M. da, Gu, W., Kim, G.-K., Koster, R., Lucchesi,  
792 R., Merkova, D., Nielsen, J. E., Partyka, G., Pawson, S., Putman, W., Rienecker, M., Schubert,  
793 S. D., Sienkiewicz, M., and Zhao, B.: The Modern-Era Retrospective Analysis for Research and  
794 Applications, Version 2 (MERRA-2), *J Climate*, 30, 5419–5454, [https://doi.org/10.1175/jcli-d-](https://doi.org/10.1175/jcli-d-16-0758.1)  
795 [16-0758.1](https://doi.org/10.1175/jcli-d-16-0758.1), 2017.
- 796  
797 Giles, D. M., Sinyuk, A., Sorokin, M. G., Schafer, J. S., Smirnov, A., Slutsker, I., Eck, T. F.,  
798 Holben, B. N., Lewis, J. R., Campbell, J. R., Welton, E. J., Korkin, S. V., and Lyapustin, A. I.:  
799 Advancements in the Aerosol Robotic Network (AERONET) Version 3 database – automated  
800 near-real-time quality control algorithm with improved cloud screening for Sun photometer  
801 aerosol optical depth (AOD) measurements, *Atmos. Meas. Tech.*, 12, 169–  
802 209, <https://doi.org/10.5194/amt-12-169-2019>, 2019.
- 803  
804 Ginoux, Paul, M Chin, I Tegen, J M Prospero, B Holben, O Dubovik, and Shian-Jiann Lin:  
805 Sources and distributions of dust aerosols simulated with the GOCART model. *J. Geophys. Res.*,  
806 106(D17), 20255–20273, 2001.
- 807 Gliß, J., A. Mortier, M. Schulz, E. Andrews, Y. Balkanski, S.E. Bauer, A.M.K. Benedictow, H.  
808 Bian, R. Checa-Garcia, M. Chin, P. Ginoux, J.J. Griesfeller, A. Heckel, Z. Kipling, A. Kirkevåg,  
809 H. Kokkola, P. Laj, P. Le Sager, M.T. Lund, C. Lund Myhre, H. Matsui, G. Myhre, D. Neubauer,  
810 T. van Noije, P. North, D.J.L. Olivié, L. Sogacheva, T. Takemura, K. Tsigaridis, and S.G. Tsyro,  
811 2021: AeroCom phase III multi-model evaluation of the aerosol life cycle and optical properties  
812 using ground- and space-based remote sensing as well as surface in situ observations. *Atmos.*  
813 *Chem. Phys.*, 21, no. 1, 87–128, doi:10.5194/acp-21-87-2021.
- 814 Gong, S. (2003) A parameterization of sea-salt aerosol source function for sub- and super-micron  
815 particles, *Global Biogeochem Cy*, 17, 1097, <https://doi.org/10.1029/2003gb002079>.
- 816 Granier, C., Bessagnet, B., Bond, T., D’Angiola, A., van der Gon, H. D., Frost, G. J., Heil, A.,  
817 Kaiser, J. W., Kinne, S., Klimont, Z., Kloster, S., Lamarque, J.-F., Liousse, C., Masui, T.,  
818 Meleux, F., Mieville, A., Ohara, T., Raut, J.-C., Riahi, K., Schultz, M. G., Smith, S. J.,  
819 Thompson, A., van Aardenne, J., van der Werf, G. R., and van Vuuren, D. P.: Evolution of  
820 anthropogenic and biomass burning emissions of air pollutants at global and regional scales  
821 during the 1980–2010 period, *Climate Change*, 109, 163–190, 2011. Grzegorski M, Poli G,  
822 Cacciari A, Jafariserajehlou S, Holdak A, Lang R, Vazquez-Navarro M, Munro R, Fournie B.  
823 Multi-Sensor Retrieval of Aerosol Optical Properties for Near-Real-Time Applications Using the  
824 Metop Series of Satellites: Concept, Detailed Description, and First Validation. *Remote Sensing*.  
825 2022; 14(1):85. <https://doi.org/10.3390/rs14010085>
- 826 Gumber, A., Reid, J. S., Holz, R. E., Eck, T. F., Hsu, N. C., Levy, R. C., Zhang, J., and Veglio,  
827 P.: Assessment of Severe Aerosol Events from NASA MODIS and VIIRS Aerosol Products for



- 828 Data Assimilation and Climate Continuity, *Atmos. Meas. Tech. Discuss.* [preprint],  
829 <https://doi.org/10.5194/amt-2022-290>, in review, 2022
- 830 Hogan, T.F. and T.E. Rosmond: The description of the Navy Operational Global Atmospheric  
831 Prediction System's spectral forecast model. *Mon. Wea. Rev.*, 119, 1786-1815, 1991.
- 832 Hogan, T. F., Liu, M., Ridout, J. S., Peng, M. S., Whitcomb, T. R., Ruston, B. C., Reynolds, C.  
833 A., Eckermann S. D., Moskaitis, J. R., Baker, N. L., McCormack, J. P., Viner, K. C., McLay, J.  
834 G., Flatau, M. K., Xu, L., Chen, C., and Chang, S. W.: The Navy Global Environmental Model.  
835 *Oceanography*, Special Issue on Navy Operational Models, 27, No. 3. 2014.
- 836 Holben, B. N., Eck, T. F., Slutsker, I., Tanre, D., Buis, J. P., Setzer, A., Vermote, E., Reagan, J.  
837 A., Kaufman, Y. J., Nakajima, T., Lavenu, F., Jankowiak, I., and Smirnov, A.: AERONET – A  
838 federated instrument network and data archive for aerosol characterization, *Remote Sens.*  
839 *Environ.*, 66, 1–16, 1998.
- 840 Hsu, N. C., Jeong, M.-J., Bettenhausen, C., Sayer, A. M., Hansell, R., Seftor, C. S., Huang, J.,  
841 and Tsay, S.-C. (2013), Enhanced Deep Blue aerosol retrieval algorithm: The second  
842 generation, *J. Geophys. Res. Atmos.*, 118, 9296– 9315, doi:[10.1002/jgrd.50712](https://doi.org/10.1002/jgrd.50712).
- 843 Hyer, E. J., Reid, J. S., and Zhang, J.: An over-land aerosol optical depth data set for data  
844 assimilation by filtering, correction, and aggregation of MODIS Collection 5 optical depth  
845 retrievals, *Atmos. Meas. Tech.*, 4, 379–408, <https://doi.org/10.5194/amt-4-379-2011>, 2011.
- 846 Ignatov, A., & Stowe, L. (2002). Aerosol Retrievals from Individual AVHRR Channels. Part I:  
847 Retrieval Algorithm and Transition from Dave to 6S Radiative Transfer Model, *Journal of the*  
848 *Atmospheric Sciences*, 59(3), 313-334. Doi: [https://doi.org/10.1175/1520-](https://doi.org/10.1175/1520-0469(2002)059<0313:ARFIAC>2.0.CO;2)  
849 [0469\(2002\)059<0313:ARFIAC>2.0.CO;2](https://doi.org/10.1175/1520-0469(2002)059<0313:ARFIAC>2.0.CO;2)
- 850 Inness, A., Ades, M., Agustí-Panareda, A., Barré, J., Benedictow, A., Blechschmidt, A.-M.,  
851 Dominguez, J. J., Engelen, R., Eskes, H., Flemming, J., Huijnen, V., Jones, L., Kipling, Z.,  
852 Massart, S., Parrington, M., Peuch, V.-H., Razinger, M., Remy, S., Schulz, M., and Suttie, M.:  
853 The CAMS reanalysis of atmospheric composition, *Atmos. Chem. Phys.*, 19, 3515–3556,  
854 <https://doi.org/10.5194/acp-19-3515-2019>, 2019.
- 855 Kahn, R. A., Gaitley, B. J., Garay, M. J., Diner, D. J., Eck, T. F., Smirnov, A., and Holben, B.  
856 N. (2010), Multiangle Imaging SpectroRadiometer global aerosol product assessment by  
857 comparison with the Aerosol Robotic Network, *J. Geophys. Res.*, 115, D23209,  
858 doi:[10.1029/2010JD014601](https://doi.org/10.1029/2010JD014601).
- 859 Kaiser, J. W., Heil, A., Andreae, M. O., Benedetti, A., Chubarova, N., Jones, L., Morcrette, J.-J.,  
860 Razinger, M., Schultz, M. G., Suttie, M., and van der Werf, G. R.: Biomass burning emis- sions  
861 estimated with a global fire assimilation system based on observed fire radiative power,  
862 *Biogeosciences*, 9, 527–554, <https://doi.org/10.5194/bg-9-527-2012>, 2012.



- 863 Kinne, S., Schulz, M., Textor, C., Guibert, S., Balkanski, Y., Bauer, S. E., Berntsen, T., Berglen,  
864 T. F., Boucher, O., Chin, M., Collins, W., Dentener, F., Diehl, T., Easter, R., Feichter, J.,  
865 Fillmore, D., Ghan, S., Ginoux, P., Gong, S., Grini, A., Hendricks, J., Herzog, M., Horowitz, L.,  
866 Isaksen, I., Iversen, T., Kirkevåg, A., Kloster, S., Koch, D., Kristjansson, J. E., Krol, M., Lauer,  
867 A., Lamarque, J. F., Lesins, G., Liu, X., Lohmann, U., Montanaro, V., Myhre, G., Penner, J.,  
868 Pitari, G., Reddy, S., Seland, O., Stier, P., Takemura, T., and Tie, X.: An AeroCom initial  
869 assessment – optical properties in aerosol component modules of global models, *Atmos. Chem.*  
870 *Phys.*, 6, 1815–1834, <https://doi.org/10.5194/acp-6-1815-2006>, 2006.  
871
- 872 Kramer, S. J., Alvarez, C., Barkley, A. E., Colarco, P. R., Custals, L., Delgado, R., Gaston, C.  
873 J., Govindaraju, R., and Zuidema, P.: Apparent dust size discrepancy in aerosol reanalysis in  
874 north African dust after long-range transport, *Atmos. Chem. Phys.*, 20, 10047–10062,  
875 <https://doi.org/10.5194/acp-20-10047-2020>, 2020.  
876
- 877 Jaegle, L., Quinn, P. K., Bates, T. S., Alexander, B., and Lin, J.-T., (2011) Global distribution of  
878 sea salt aerosols: new constraints from in situ and remote sensing observations, *Atmos Chem*  
879 *Phys.*, 11, 3137–3157, <https://doi.org/10.5194/acp-11-3137-2011>.
- 880 Jenwitheesuk, K.; Peansukwech, U.; Jenwitheesuk, K., (2022) Predictive MERRA-2 aerosol  
881 diagnostic model for oral, oropharyngeal and laryngeal cancer caused by air pollution in Thai  
882 population, *Toxicology Reports*, 9, 970–978. Doi: <https://doi.org/10.1016/j.toxrep.2022.04.015>.  
883
- 884 Lacima, A., Petetin, H., Soret, A., Bowdalo, D., Jorba, O., Chen, Z., Méndez Turrubiates, R. F.,  
885 Achebak, H., Ballester, J., and Pérez García-Pando, C.: Long-term evaluation of surface air  
886 pollution in CAMSRA and MERRA-2 global reanalyses over Europe (2003–2020), *Geosci.*  
887 *Model Dev. Discuss.* [preprint], <https://doi.org/10.5194/gmd-2022-197>, in review, 2022.  
888
- 889 Levy, R. C.; Mattoo, S.; Munchak, L. A.; Remer, L. A.; Sayer, A. M.; Patadia, F.; Hsu, N. C.  
890 The Collection 6 MODIS aerosol products over land and ocean, *Atmos. Meas. Tech.*, 2013, 6,  
891 2989–3034, <https://doi.org/10.5194/amt-6-2989-2013>.  
892
- 893 Lynch, P., Reid, J. S., Westphal, D. L., Zhang, J., Hogan, T. F., Hyer, E. J., Curtis, C. A., Hegg,  
894 D. A., Shi, Y., Campbell, J. R., Rubin, J. I., Sessions, W. R., Turk, F. J., and Walker, A. L.: An  
895 11-year global gridded aerosol optical thickness reanalysis (v1.0) for atmospheric and climate  
896 sciences, *Geosci. Model Dev.*, 9, 1489–1522, <https://doi.org/10.5194/gmd-9-1489-2016>, 2016.
- 897 McCoy, D. T., F. A.-M. Bender, J. K. C. Mohrmann, D. L. Hartmann, R. Wood, and D. P.  
898 Grosvenor (2017): The global aerosol-cloud first indirect effect estimated using MODIS,  
899 MERRA, and AeroCom, *J. Geophys. Res. Atmos.*, 122, 1779–1796, doi:10.1002/2016JD026141.
- 900 Monahan, E. C., Spiel, D. E., and Davidson, K. L.: A model of marine aerosol generation via  
901 whitecaps and wave disruption, in *Oceanic Whitecaps*, edited by: Monahan, E. and Niocaill, G.  
902 M., D. Reidel, Norwell, Mass., 167–174, 1986.
- 903 Ningombam, Shantikumar S., Dumka, Umesh Chandra, Mugil, Sivasamy Kalamani, Kuniyal,  
904 Jagdish Chandra, Hooda, Rakesh K., Gautam, Alok Sagar, and Tiwari, Suresh, 2021, "Impacts of



- 905 Aerosol Loading in the Hindu Kush Himalayan Region Based on MERRA-2 Reanalysis Data"  
906 Atmosphere Vol. 12, No. 10, pp 1290, 2073-4433
- 907 Ohno, T., Irie, H., Momoi, M. and da Silva, A.M. : Quantitative evaluation of mixed biomass  
908 burning and anthropogenic aerosols over the Indochina Peninsula using MERRA-2 reanalysis  
909 products validated by sky radiometer and MAX-DOAS observations. Prog Earth Planet Sci 9, 61  
910 (2022). <https://doi.org/10.1186/s40645-022-00520-4>
- 911  
912 O'Neill, N.T., Eck, T. F., Holben, B. N., Smirnov, A., Dubovik, O. and Royer, A.: Bimodal size  
913 distribution influences on the variation of Angstrom derivatives in spectral and optical depth  
914 space, J. Geophys. Res., 106, 9787-9806, 2001.
- 915  
916 O'Neill, N. T., Eck, T. F., Smirnov, A., Holben, B. N., and Thulasiraman, S.: Spectral  
917 discrimination of coarse and fine mode optical depth. J. Geophys. Res., 108, D05212,  
918 doi:10.1029/2002JD002975, 2003.
- 919  
920 O'Sullivan, D., Marengo, F., Ryder, C. L., Pradhan, Y., Kipling, Z., Johnson, B., Benedetti, A.,  
921 Brooks, M., McGill, M., Yorks, J., and Selmer, P.: Models transport Saharan dust too low in the  
922 atmosphere: a comparison of the MetUM and CAMS forecasts with observations, Atmos. Chem.  
923 Phys., 20, 12955–12982, <https://doi.org/10.5194/acp-20-12955-2020>, 2020.
- 924
- 925 Randles, C. A., daSilva, A. M., Buchard, V., Colarco, P. R., Darmenov, A., Govindaraju, R., et  
926 al.: The MERRA-2 aerosol reanalysis, 1980 onward. Part I: System description and data  
927 assimilation evaluation. Journal of Climate, 30(17), 6823-6850. [https://doi.org/10.1175/JCLI-D-](https://doi.org/10.1175/JCLI-D-16-0609.1)  
928 [16-0609.1](https://doi.org/10.1175/JCLI-D-16-0609.1), 2017.
- 929 Reid, J.S., Gumber, A. ; Zhang, J.; Holz, R. E.; Rubin, J. I.; Xian, P.; Smirnov, A.; Eck, T. F. ;  
930 O'Neill, N. T.; Levy, R. C.; Reid, E. A.; Colarco, P. R.; Benedetti, A.; and Tanaka, T. (2022) A  
931 Coupled Evaluation of Operational MODIS and Model Aerosol Products for Maritime  
932 Environments Using Sun Photometry: Evaluation of the Fine and Coarse Mode. Remote Sens,  
933 14, 2978. <https://doi.org/10.3390/rs14132978>.
- 934 Reid, J. S., and Coauthors, 2023: The coupling between tropical meteorology, aerosol lifecycle,  
935 convection, and radiation, during the Cloud, Aerosol and Monsoon Processes Philippines  
936 Experiment (CAMP2Ex). Bull. Amer. Meteor. Soc., E1179-E1205,  
937 <https://doi.org/10.1175/BAMS-D-21-0285.1>
- 938 Reid, J. S., Hyer, E. J., Prins, E. M., Westphal, D. L., Zhang, J., Wang, J., Christopher, S. A.,  
939 Curtis, C. A., Schmidt, C. C., Eleuterio, D. P., Richardson, K. A., and Hoffman, J. P.: Global  
940 Monitoring and Forecasting of Biomass-Burning Smoke: Description of and Lessons from the  
941 Fire Locating and Modeling of Burning Emissions (FLAMBE) Program, IEEE J. Sel. Top.  
942 Appl., 2, 144–162, JSTARS-2009-00034, 2009.
- 943 Reid, J. S., Xian, P., Hyer, E. J., Flatau, M. K., Ramirez, E. M., Turk, F. J., Sampson, C. R.,  
944 Zhang, C., Fukada, E. M., and Maloney, E. D.: Multi-scale meteorological conceptual analysis of



- 945 observed active fire hotspot activity and smoke optical depth in the Maritime Continent, *Atmos.*  
946 *Chem. Phys.*, 12, 2117–2147, <https://doi.org/10.5194/acp-12-2117-2012>, 2012.
- 947 Reid, J. S., Xian, P., Holben, B. N., Hyer, E. J., Reid, E. A., Salinas, S. V., Zhang, J., Campbell,  
948 J. R., Chew, B. N., Holz, R. E., Kuciauskas, A. P., Lagrosas, N., Posselt, D. J., Sampson, C. R.,  
949 Walker, A. L., Welton, E. J., and Zhang, C.: Aerosol meteorology of the Maritime Continent for  
950 the 2012 7SEAS southwest monsoon intensive study – Part 1: regional-scale phenomena, *Atmos.*  
951 *Chem. Phys.*, 16, 14041–14056, <https://doi.org/10.5194/acp-16-14041-2016>, 2016.
- 952 Roychoudhury, C., He, C., Kumar, R., McKinnon, J. M., & Arellano, A. F. Jr. (2022). On the  
953 relevance of aerosols to snow cover variability over High Mountain Asia. *Geophysical Research*  
954 *Letters*, 49, e2022GL099317. <https://doi.org/10.1029/2022GL099317>
- 955 Sayer, A.M., Munchak, L.A., Hsu, N.C., Levy, R.C., Bettenhausen, C., Jeong, M.J., 2014.  
956 MODIS Collection 6 aerosol products: comparison between Aqua’s e-Deep Blue, Dark Target,  
957 and “merged” \_data sets, and usage recommendations. *J. Geophys. Res. Atmos.* 119 (24), 13–  
958 965.
- 959 Schutgens, N., Sayer, A. M., Heckel, A., Hsu, C., Jethva, H., de Leeuw, G., Leonard, P. J. T.,  
960 Levy, R. C., Lipponen, A., Lyapustin, A., North, P., Popp, T., Poulsen, C., Sawyer, V.,  
961 Sogacheva, L., Thomas, G., Torres, O., Wang, Y., Kinne, S., Schulz, M., and Stier, P.: An  
962 AeroCom–AeroSat study: intercomparison of satellite AOD datasets for aerosol model  
963 evaluation, *Atmos. Chem. Phys.*, 20, 12431–12457, <https://doi.org/10.5194/acp-20-12431-2020>,  
964 2020.  
965
- 966 Shi, Y., Zhang, J., Reid, J. S., Hyer, E. J., and Hsu, N. C.: Critical evaluation of the MODIS  
967 Deep Blue aerosol optical depth product for data assimilation over North Africa, *Atmos. Meas.*  
968 *Tech.*, 6, 949–969, <https://doi.org/10.5194/amt-6-949-2013>, 2013.  
969
- 970 Shi, Y., Zhang, J., Reid, J. S., Holben, B., Hyer, E. J., and Curtis, C.: An analysis of the  
971 collection 5 MODIS over-ocean aerosol optical depth product for its implication in aerosol  
972 assimilation, *Atmos. Chem. Phys.*, 11, 557–565, <https://doi.org/10.5194/acp-11-557-2011>, 2011.  
973
- 974 Sorenson, B. T., Zhang, J., Reid, J. S., Xian, P., and Jaker, S. L.: Ozone Monitoring Instrument  
975 (OMI) UV aerosol index data analysis over the Arctic region for future data assimilation and  
976 climate forcing applications, *Atmos. Chem. Phys.*, 23, 7161–7175, <https://doi.org/10.5194/acp-23-7161-2023>, 2023.  
977  
978
- 979 Textor, C., Schulz, M., Guibert, S., Kinne, S., Balkanski, Y., Bauer, S., Berntsen, T., Berglen, T.,  
980 Boucher, O., Chin, M., Dentener, F., Diehl, T., Easter, R., Feichter, H., Fillmore, D., Ghan, S.,  
981 Ginoux, P., Gong, S., Grini, A., Hendricks, J., Horowitz, L., Huang, P., Isaksen, I., Iversen, I.,  
982 Kloster, S., Koch, D., Kirkevåg, A., Kristjansson, J. E., Krol, M., Lauer, A., Lamarque, J. F., Liu,  
983 X., Montanaro, V., Myhre, G., Penner, J., Pitari, G., Reddy, S., Seland, Ø., Stier, P., Takemura,  
984 T., and Tie, X.: Analysis and quantification of the diversities of aerosol life cycles within  
985 AeroCom, *Atmos. Chem. Phys.*, 6, 1777–1813, <https://doi.org/10.5194/acp-6-1777-2006>, 2006.  
986



- 987 Tong, D. Q., et al., Health and Safety Effects of Airborne Soil Dust in the Americas and Beyond.  
988 Reviews of Geophysics. <https://doi.org/10.1029/2021RG000763>  
989
- 990 Xian, P., Klotzbach, P. J., Dunion, J. P., Janiga, M. A., Reid, J. S., Colarco, P. R., and Kipling,  
991 Z.: Revisiting the relationship between Atlantic dust and tropical cyclone activity using aerosol  
992 optical depth reanalyses: 2003–2018, Atmos. Chem. Phys., 20, 15357–15378,  
993 <https://doi.org/10.5194/acp-20-15357-2020>, 2020.  
994
- 995 Xian, P., Reid J. S., Hyer, E., Sampson, C.R., Rubin, J., Ades M., et. al., Current state of the  
996 global operational aerosol multi-model ensemble: an update from the International Cooperative  
997 for Aerosol Prediction (ICAP), Quarterly J. of the Royal Met. Soc.  
998 <https://doi.org/10.1002/qj.3497>, 2019.  
999
- 1000 Xian, P., Reid, J. S., Turk, J. F., Hyer, E. J., and Westphal, D. L.: Impact of models versus  
1001 satellite measured tropical precipitation on regional smoke optical thickness in an aerosol  
1002 transport model, Geophys. Res. Lett., 36, L16805, doi:10.1029/2009GL038823, 2009.  
1003
- 1004 Xian, P., Reid, J. S., Atwood, S. A., Johnson, R. S., Hyer, E. J., Westphal, D. L., Sessions, W.:  
1005 Smoke aerosol transport patterns over the Maritime continent, Atmos. Res. Vol. 122, 469-485,  
1006 <https://doi.org/10.1016/j.atmosres.2012.05.006>
- 1007 Xian, P., Zhang, J., O'Neill, N. T., Toth, T. D., Sorenson, B., Colarco, P. R., Kipling, Z., Hyer, E.  
1008 J., Campbell, J. R., Reid, J. S., and Ranjbar, K.: Arctic spring and summertime aerosol optical  
1009 depth baseline from long-term observations and model reanalyses – Part 1: Climatology and  
1010 trend, Atmos. Chem. Phys., 22, 9915–9947, <https://doi.org/10.5194/acp-22-9915-2022>, 2022.
- 1011 Witek, M. L., P. J. Flatau, P. K. Quinn, and D. L. Westphal: Global sea-salt modeling: Results  
1012 and validation against multicampaign shipboard measurements, J. Geophys. Res., 112, 2007.
- 1013 Yumimoto, K., Tanaka, T. Y., Oshima, N., and Maki, T.: JRAero: the Japanese Reanalysis for  
1014 Aerosol v1.0, Geosci. Model Dev., 10, 3225–3253, <https://doi.org/10.5194/gmd-10-3225-2017>,  
1015 2017.
- 1016 Yukimoto, S., Adachi, Y., Hosaka, M., Sakami, T., Yoshimura, H., Hirabara, M., Tanaka, T. Y.,  
1017 Shindo, E., Tsujino, H., Deushi, M., Mizuta, R., Yabu, S., Obata, A., Nakano, H., Koshiro, T.,  
1018 Ose, T., and Kitoh, A.: A New Global Climate Model of the Meteorological Research Institute:  
1019 MRI-CGCM3 –Model Description and Basic Performance, J. Meteorol. Soc. Jpn., 90A, 23–64,  
1020 <https://doi.org/10.2151/jmsj.2012-A02>, 2012.
- 1021 Zhang, J. L., and J. S. Reid: MODIS aerosol product analysis for data assimilation: Assessment  
1022 of over-ocean level 2 aerosol optical thickness retrievals. J. Geophys. Res.-Atmos., 111, 2006.  
1023
- 1024 Zhang, J. L., and Reid, J. S., Westphal, D. L., Baker, N. L., and Hyer, E. J.: A system for  
1025 operational aerosol optical depth data assimilation over global oceans. J. Geophys. Res., 113,  
1026 D10208, doi:10.1029/2007JD009065, 2008.  
1027



- 1028 Zhang J., Reid, J. S., Alfaro-Contreras, R., Xian P., Has China been exporting less particulate air  
1029 pollution over the past decade?, *Geophysical Research Letters*, 10.1002/2017GL072617, 2017.  
1030
- 1031 Zhang, J., Spurr, R. J. D., Reid, J. S., Xian, P., Colarco, P. R., Campbell, J. R., Hyer, E. J., and  
1032 Baker, N. L.: Development of an Ozone Monitoring Instrument (OMI) aerosol index (AI) data  
1033 assimilation scheme for aerosol modeling over bright surfaces – a step toward direct radiance  
1034 assimilation in the UV spectrum, *Geosci. Model Dev.*, 14, 27–42, [https://doi.org/10.5194/gmd-](https://doi.org/10.5194/gmd-14-27-2021)  
1035 [14-27-2021](https://doi.org/10.5194/gmd-14-27-2021), 2021.  
1036
- 1037 Zhang, X., and Zhou, Y.: Aerosol direct radiative forcing over China: A 40-year MERRA-2-  
1038 based evaluation, *Atmos. Env.*, Vol., 299, <https://doi.org/10.1016/j.atmosenv.2023.119659>